Genome Biology

RESEARCH

Open Access

# ASPM mediates nuclear entrapment of FOXM1 via liquid-liquid phase separation to promote progression of hepatocarcinoma

Xunliang Jiang[1,2,3†], Jun Liu[2†], Ke Wang[2,4†], Jianyong Sun[2,5†], Huilong Yin[2,6], Yu Jiang[2,7], Yongkang Liu[2], Ningbo Wang[2], Xiaochen Ding[8], Pu Gao[9], Lin Li[2], Xiang Zhang[2,10*], Jipeng Li[1,3,8*] and Rui Zhang[2,11*]

†Xunliang Jiang, Jun Liu, Ke Wang and Jianyong Sun contributed equally to this work.

*Correspondence: biozx@fmmu.edu.cn; jipengli1974@aliyun.com; ruizhang@fmmu.edu.cn

[1] State Key Laboratory of Holistic Integrative Management of Gastrointestinal Cancers, National Clinical Research Center for Digestive Diseases and Xijing Hospital of Digestive Diseases, Fourth Military Medical University, Xi'an 710032, China
[2] State Key Laboratory of Holistic Integrative Management of Gastrointestinal Cancers, Department of Biochemistry and Molecular Biology, Fourth Military Medical University, Xi'an 710032, China
Full list of author information is available at the end of the article

## Abstract

**Background:** Fork-head box protein M1 (FOXM1) plays critical roles in development and progression of multiple cancers, including hepatocellular carcinoma (HCC). However, the exact regulatory hierarchy of FOXM1 remains unclear. Here, a genome-wide screen is performed to identify intranuclear proteins that promote FOXM1 transcription activity via liquid–liquid phase separation (LLPS).

**Results:** Abnormal spindle-like microcephaly associated (ASPM) is identified to interact with FOXM1 protein via LLPS and enhance its stability by preventing proteasome-mediated degradation. ChIP-sequencing data show ASPM and FOXM1 co-occupy the promoters of multiple genes to promote their transcription, enhancing FOXM1-driven oncogenic progression. In functional experiments, inhibition of ASPM suppresses tumor growth of HCC cells in vivo and in vitro, while overexpression of ASPM has opposite effects. Importantly, reconstitution of FOXM1 partially compensates for the weakened proliferative capacity of HCC cells caused by ASPM silencing. Intriguingly, FOXM1 binds to the promoter region of ASPM and transcriptionally activates ASPM expression in HCC cells. Furthermore, we find that a higher co-expression of ASPM and FOXM1 significantly correlates with poor prognosis in HCC patients. It indicates a double positive feedback loop between ASPM and FOXM1 which coordinately promotes the aggressive progression of HCC.

**Conclusions:** Collectively, we demonstrate that LLPS and transcriptional regulation form an oncogenic double positive feedback loop between ASPM and FOXM1. This provides a rationale strategy to treat HCC by targeting this mechanism.

**Keywords:** Human hepatocellular carcinoma, Double positive feedback loop, Liquid–liquid phase separation, FOXM1, Protein degradation

## Background

Hepatocellular carcinoma (HCC) is the sixth-most diagnosed cancer and the third major reason of cancer-associated death worldwide in 2020 [1]. Imbalance of gene regulation disrupts the homeostasis in liver tissues [2]. In the past decades, a series of transcription factors, such as c-Myc, YAP1, FOXM1 et al., have been demonstrated to be critical in HCC pathogenesis [3]. However, the therapeutics based on transcription factors are still lack and difficult to exploit in HCC [4].

Liquid–liquid phase separation (LLPS) describes the spontaneous demixing of a homogeneous solution into two or more distinct phases. It occurs when interactions among subsets of molecules overcome the tendency to remain disordered in solution, causing these molecules to become enriched in the demixed (condensed) phase and depleted from the bulk (diffuse) solution [5]. These molecules often exhibit a sticker-and-spacer configuration [6]. Stickers, also known as domains/motifs interacted with other biomolecules, are multiple folded binding modules and/or short interaction sequences. Spacers, also known as intrinsically disordered regions (IDR) in LLPS, are often unfolded or disordered. "Stickers" are usually separated by "spacers" within a molecule, achieving multivalency while promoting liquid-like behaviors [5, 6]. During the LLPS process between proteins with sticker-and-spacer configuration, noncovalent interactions between "stickers" within and from different proteins will lead to the formation of reversible physical crosslinks firstly, and then the "spacers" hinged together [6]. It suggests that protein–protein interaction analysis (e.g., molecular docking) remains valuable in prediction of LLPS between intrinsically disordered proteins (IDPs).

LLPS is widely observed to directly regulate key cellular processes, including transcriptional regulation [7], proteasomal degradation [8], and so on. Although Trojanowski et al. claimed that transcription activation is enhanced by multivalent interactions independent of phase separation [9], more and more papers illustrated LLPS are involved in transcriptional regulation, especially toward transcriptional activation [10–12]. Boija A et al. found that, under physiological conditions, activation domains from multiple transcription factors form phase-separated condensates with mediator to activate gene expression [10]. Zhang et al. demonstrated that, during acute stress, heat-shock transcription factor 1 (HSF1) forms LLPS condensates at heat-shock-protein gene loci and promotes their transcription [11]. Recently, Liu et al. uncovered the feasibility of using phase-separation proteins to assist in the enhancement of gene expression, via developing CRISPR-assisted transcription activation system by phase-separation proteins [12]. In HCC, Liu et al. reported that accumulated glycogen undergoes phase separation to suppress Hippo signaling in HCC-initiating cells [13]. However, more mechanisms of LLPS involved in development and progression of HCC are still unclear.

Forkhead box protein M1 (FOXM1) is a member of the forkhead box transcription factor family that plays critical roles in mitosis, DNA damage repair, and tissue regeneration by binding to classical binding motifs on the promoter region of target genes and transactivating downstream genes [14, 15]. In recent years, a growing body of evidence has demonstrated that FOXM1 widely regulates multiple malignant behaviors in cancers, including unlimited cancer cell proliferation, radiotherapy and chemotherapy resistance, metabolic reprogramming, angiogenesis, and so on [16]. It has been documented that FOXM1 is essential for development and progression of many types of solid

tumors. Aberrantly high activation of a FOXM1-driven signaling is frequently associated with poor prognosis in cancer patients [16]. Recently, in the process of deeply understanding the underlying mechanism of FOXM1-driven oncogenic progression, it was reported that FOXM1 cooperates with oncogenic transcription factor YAP1 to contribute to chromosome instability in hepatocarcinogenesis [17]. In addition, we also showed that FOXM1-mediated transcriptional activation of CCNB1 and STMN1 could be the more precise biomarkers for prognostic prediction in human hepatocellular carcinoma [18, 19]. Collectively, the global identification of the FOXM1-involved network provides a significant guidance for clinical application including prognostic analysis and cancer treatment. However, on the other side of a coin, the upstream regulatory mechanism of FOXM1 itself is still an open issue waiting for absolute investigation.

The abnormal spindle-like microcephaly associated (ASPM), the human ortholog of the *Drosophila melanogaster* "abnormal spindle" gene (asp), encodes ASPM which localizes at the centrosome of apical neuro progenitor cells and is involved in spindle pole positioning during neurogenesis [20]. Loss-of-function mutations in ASPM are associated with microcephaly primary type 5, which affects the majority of all microcephaly primary hereditary (MCPH) patients worldwide [21]. In addition, ASPM, as a scaffold protein, promotes the recruitment of TopBP1 and RAD9 on replication forks, thus promoting the activation of ATR-CHK1 signal axis under replication stress. At the same time, ASPM recruited blocked replication forks to protect newly synthesized DNA strands from being degraded by nuclease MRE11, thus maintaining the stability of replication forks and ensuring the stability of genome to avoid the occurrence of tumors and other diseases [22]. Strikingly, a large number of works in recent years have reported that an aberrantly high level of ASPM is a biomarker for aggressive progression and poor prognosis in many types of solid tumors, including liver cancer [23], gastric cancer [24], pancreatic cancer [25], prostate cancer [26], and glioma [27]. Among all documented types of cancers, HCC was firstly reported to be related with ASPM [23]. It was found that a high level of ASPM is an indicator of vascular invasion, early recurrence, and poor prognosis in HCC [23]. However, the functional role and regulatory mechanism of ASPM in malignant diseases are still ambiguous. Until recently, it has been identified that ASPM isoforms showed remarkably different subcellular location. Specifically, ASPM-iI is exclusively localized to the cytoplasm of pancreatic cancer cells and gastric cancer cells, while ASPM-iII is predominantly expressed in the cellular nucleus [28]. Mechanistically, Tsai Lab identified that cytoplasm-localized ASPM isoform interacts with disheveled (Dvl) family members to augment β-catenin-dependent oncogenic activation [24–26, 29]. Importantly, the amino acid sequence of ASPM-iII contains three specific nuclear localization signals and is thought to selectively regulate the expression of cell cycle-related molecules in the cellular nucleus to promote cell proliferation [30]. Most cell cycle-related molecules are believed to be closely associated with tumorigenesis and progress in malignant disease. However, as an important participant in cell cycle progression, how cellular nucleus-localized ASPM regulates tumorigenesis and aggressive progress in HCC has not been clearly reported.

In this study, we identify that ASPM physically interacts with FOXM1 and induces liquid–liquid phase separation in the cellular nuclei of HCC cells, leading to increased stability of FOXM1 proteins by preventing proteasome-mediated degradation.

Furthermore, ASPM and FOXM1 coordinately promote a FOXM1-driven oncogenic progression in HCC cells. Intriguingly, FOXM1 transcriptionally activates the expression of ASPM. These findings indicate that a double positive feedback loop between ASPM and FOXM1 coordinately promotes the aggressive progression in HCC.

## Results

### A genome-wide screen identifies potential intranuclear partner components in phase separation for boosting FOXM1 during hepatocellular carcinoma progression

To investigate significance of nuclear translocation of FOXM1 in the progression of hepatocellular carcinoma, we collected HCC tissues with different stages and adjacent normal tissues from the clinic (Additional file 1: Table S1). Immunohistochemical (IHC) staining assays displayed that H-Score ratio between nuclear and total FOXM1 significantly elevated with advanced progression of HCC (Fig. 1A, Additional file 1: Fig. S1A). Previous studies reported that nuclear translocation of FOXM1 is mediated by a serial of kinases, such as CDK4/6 and PLK1 [31, 32]; however, none of them were elevated significantly with advanced progression of HCC by bioinformatic analysis in TCGA-LIHC data (Additional file 1: Fig. S1B). Accordingly, some unknown mechanisms might be involved in nuclear localization of FOXM1 in HCC.

It has been demonstrated that liquid–liquid phase separation drives cellular function and dysfunction in cancers by forming intracellular biomolecular condensates, especially in the nucleus [5, 33, 34]. We supposed that phase separation might be involved in FOXM1 transcription activity and consequent progression of HCC in the nucleus, and we performed a genome-wide screen as depicted in Fig. 1B. All 5654 nucleus-located genes were screened by GSEA assays one by one, and 175 genes were positively relative to a widely accepted FOXM1 downstream gene set [35]. Then, all the 175 candidate genes were evaluated by PhaSePred [36], an online meta-predictor for phase-separating proteins, 5 genes were filtered out with high partner-dependent phase-separating (PS-Part) score and low self-assembling phase-separating (PS-Self) score. Among them,

(See figure on next page.)

**Fig. 1** A genome-wide screen identifies ASPM involved in phase separation of FOXM1 in nucleus and promoting transcription activity of FOXM1 in HCC. **A** Relative FOXM1 signaling between nuclear and total cells in different-stage clinical HCC samples by immunohistochemical staining assays. **B** Schematic depiction of the genome-wide screen. All 5654 nucleus-located genes (data from Uniprot) were screened by GSEA assays one by one, and 175 genes were positively relative to a widely accepted FOXM1 downstream gene set. Then, all the 175 genes were evaluated by PhaSePred, an online meta-predictor for phase-separating proteins, 5 genes were filtered out with high partner-dependent phase-separating (PS-Part) scores and low self-assembling phase-separating (PS-Self) scores. **C** Confocal microscopy images of condensates formation in cells after transfection GFP-FOXM1 and indicated genes. The scale bar is 5 μm. **D** The expression plasmids ASPM-mCherry and FOXM1-GFP were co-transfected in HEK-293 T cells. Co-IP experiments were performed to test the interaction of these two molecules. After immunoprecipitation with an anti-mCherry tag or anti-GFP tag antibody, the immunoprecipitation was analyzed for mCherry(-ASPM) and GFP(-FOXM1) by immunoblotting, respectively. **E** The localization of ASPM and FOXM1 in HCC tissues was analyzed by immunofluorescence. The nuclei (blue) were stained with DAPI, the ASPM (green) was labeled with Alexa Fluor 488, and the FOXM1 (red) was labeled with Alexa Flour 555. The scale bars are 50 μm (top) and 10 μm (bottom). **F** Molecular docking analysis between ASPM and DNA binding domain (DBD) of FOXM1 by ClusPro server. **G** Genomic distribution and top enriched motifs of ASPM ($n = 437{,}295$) ChIP-seq peaks in HepG2 cells. **H** Genomic distribution and top enriched motifs of FOXM1 ($n = 159{,}359$) ChIP-seq peaks in HepG2 cells. **I** Venn diagrams showing overlap between ASPM-associated and FOXM1-associated genes in ChIP-seq

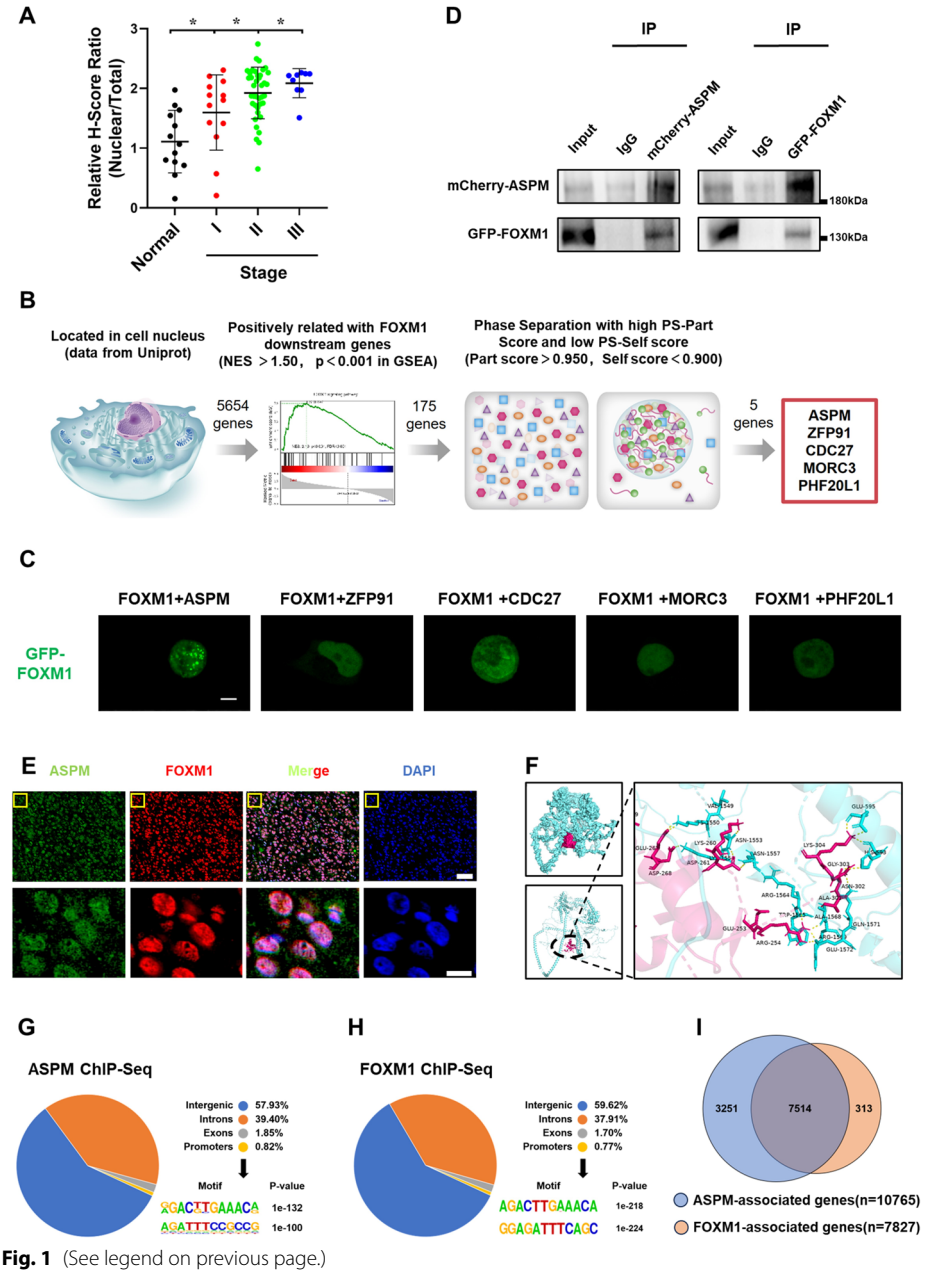


**Fig. 1** (See legend on previous page.)

ASPM, the abnormal spindle-like microcephaly-associated protein, ranked one of the top candidates (Additional file 1: Table S2). Furthermore, these 5 candidate genes were co-transfected with GFP-FOXM1 in HEK-293 T cells, respectively, and only Aspm-iII (the isoform located in nucleus, named ASPM in short later) triggered condensates formation of FOXM1 in the nucleus (Fig. 1C). It indicated that ASPM might play a critical role in triggering LLPS of FOXM1 in HCC.

Furthermore, we performed co-immunoprecipitation (co-IP) assays to investigate whether ASPM interacts with FOXM1 in HCC. As shown in Fig. 1D and Additional file 1: Fig. S1C, ASPM and FOXM1 interact with each other in HCC cells and tumor tissues, respectively. In addition, data of the immunofluorescent staining also showed

obviously co-localization of ASPM and FOXM1 in the cellular nucleus. It was not only in HCC cell lines (Additional file 1: Fig. S1D), but also in sections from clinical tumor samples (Fig. 1E). Given that the crystal structure of ASPM has not been resolved, we predicted it by AlphaFold, a powerful tool that could predict protein structure closely to crystal structure data [37, 38]. Then, the molecular docking assay testing interaction between ASPM and FOXM1 was performed by ClusPro, and the molecular visualization results showed that there are dozens of amino acid residues of ASPM that is involved in binding to residues in FOXM1 through hydrogen bond interactions (Fig. 1F, Additional file 1: Fig. S2C and Additional file 1: Table S3). Above results indicated that ASPM can interact directly with FOXM1 in nuclei of HCC cells. More importantly, analysis of nuclear and cytoplasmic fractions showed that knockdown of ASPM decreases the ratio of nuclear to cytoplasmic FOXM1 (Additional file 1: Fig. S1E-F), while overexpression of ASPM increases the ratio of nuclear to cytoplasmic FOXM1 in HCC cells (Additional file 1: Fig. S1G).

Next, we wondered if interaction between ASPM and FOXM1 can promote FOXM1-driven gene expression. Given that ASPM has no obviously known DNA binding domain, if ASPM could interact with FOXM1 and promote FOXM1's transcriptional activity, these two molecules should have the similar pattern on the genomic occupancy. Thus, we performed ChIP-seq assay in HCC cells by using ASPM and FOXM1 antibody, respectively. As shown in Fig. 1G, H, a total of 437,295 binding peaks (10,765 genes involved) were detected in the ASPM ChIP-seq data and 159,359 peaks (7827 genes involved) in the FOXM1 group. As expected, the genomic distribution and Gene Ontology (GO) enrichment analysis of ASPM and FOXM1 binding peaks were significantly similar (Fig. 1G, H and Additional file 1: Fig. S1H). Importantly, the great majority of ASPM annotated genes overlapped with FOXM1-bound genes (F1g. 1I), and the classical binding motif of FOXM1 was also found among the predicted binding motifs of ASPM (Fig. 1G, H). Furthermore, we then performed ChIP-qPCR to test the predicted downstream genes that can be coordinatively regulated by ASPM and FOXM1 in HepG2 cancer cells. As shown in Additional file 1: Fig. S1I, the binding capacity of ASPM on the genomic loci of CCNE1 and SOX2, classical downstream genes of FOXM1, is significantly dampened with the downregulation of endogenous FOXM1 expression.

Taken together, ASPM was screened and confirmed to interact with FOXM1 and augments its transactivation in the human hepatocellular carcinoma cells.

#### FOXM1 interacts and forms dynamic condensates with ASPM

To investigate whether the interaction of FOXM1 and ASPM trigger liquid–liquid phase separation, we conducted super-resolution microscopic observations on cells transfected with green fluorescent protein-FOXM1 (GFP-FOXM1) and mCherry-ASPM. Compared to cells transfected with GFP-FOXM1 or mCherry-ASPM alone, cells transfected with GFP-FOXM1 and mCherry-ASPM showed more significant droplet-like condensates in the nuclei (Fig. 2A, B). Compared with solid-like condensates, liquid-like condensates are more dynamic with rapid fluorescence recovery after photo bleaching (FRAP). Live-cell imaging revealed discrete nuclear puncta in the region of FOXM1-ASPM droplets (Fig. 2B right). These FOXM1-ASPM puncta recovered fluorescence rapidly and exhibited liquid–liquid-like properties (Fig. 2C). Super resolution imaging showed that

endogenous FOXM1 and ASPM formed small condensates in cells, and colocalized condensates were observed. Removing either FOXM1 or ASPM significantly affected the formation of the condensates (Fig. 2D). These data identified the dynamic and reversible properties of FOXM1-ASPM condensates in cells.

Next, to explore the structural basis of FOXM1-ASPM condensates, we analyzed the amino acid sequences of the two proteins (Fig. 2E and Additional file 1: Fig. S2A-B). The N- and C-terminal of FOXM1 and the N-terminal of ASPM were predicted as intrinsic disordered regions (IDRs). As shown in the confocal microscopy assay, either the depletion of IDRs in FOXM1 or ASPM disrupted condensate formation, indicating that the predicted IDRs contribute to phase separation of ASPM and FOMX1 in HCC cells (Fig. 2F). Furthermore, the absence of predicted FOXM1 interaction region impaired condensate formation (FOXM1 N-IDR and FOXM1 C-IDR, in Fig. 2E, F), indicating that the interaction between FOXM1 and ASPM is essential for condensate formation.

To further confirm the biological contribution of ASPM on LLPS of FOXM1, we fused IDR of ASPM to the N-terminal of CDK6, a FOXM1 interacting protein. As shown in Fig. 2G, CDK6 alone did not trigger condensate formation of GFP-FOXM1, while the fusion protein of CDK6 and ASPM IDR triggered condensate formation of GFP-FOXM1 in HEK-293 T cells. Collectively, these observations revealed a multivalent interaction model that the interaction between the FOXM1 and ASPM is a prerequisite for condensate initiation, and the weak promiscuous interactions between the IDRs of both FOXM1 and ASPM promote condensate formation.

#### ASPM enhances FOXM1 protein stability by preventing proteasome-mediated degradation

To further identify the regulatory mechanism of ASPM on FOXM1, we used two independent siRNAs to knock down ASPM in SNU-739 and HepG2 cell lines (Additional file 1: Fig. S3A-B). As shown in Fig. 3A, knockdown of ASPM reduced the protein level of FOXM1 in SNU-739 and HepG2 cells; furthermore, significant decrease also be observed in classic downstream genes of FOXM1, such as Cyclin E1, SOX2 (Fig. 3B). However, there is no obvious change on the RNA level of FOXM1 in both tested cell lines (Fig. 3C), indicating that ASPM-mediated regulation FOXM1 may be in a post-transcriptional manner.

(See figure on next page.)

**Fig. 2** FOXM1 interacts and forms dynamic condensates with ASPM. **A** Confocal microscopy images of condensate formation in HepG2 cells. The scale bar is 2 μm. **B** Line scan analysis results of fluorescence intensity along the indicated lines in Fig. 2 A are shown. **C** Top: quantification of FRAP data for GFP-FOXM1 droplets. The bleaching event occurs at $t = 0$ s. Mean ± SEM. $n = 3$. Bottom: representative images of fluorescence recovery. The scale bar is 2 μm. **D** TOP: structured illumination microscopy analysis of endogenous FOXM1 and ASPM localization in HepG2 cells. Middle and bottom: the fluorescence images with knocking down FOXM1 or ASPM. The scale bar is 5 μm. **E** Protein structure and IDR analysis of FOXM1 (left) and ASPM (right). The scores above 0.5 indicate disorder. The representative diagrams indicating the major domains of full-length FOXM1 and ASPM and the truncated constructs are shown below. FL, full length; DB, DNA binding; IDR, intrinsically disordered regions; CH, Calponin-homology; IQ, IQ protein domain. **F** Confocal microscopy images of condensates formation in HepG2 cells transfected with the indicated constructs. Line scan analysis results of fluorescence intensity along the indicated lines are shown on the right. The scale bar is 5 μm. **G** Confocal microscopy images of condensates formation in HepG2 cells transfected with GFP-FOXM1 and indicated constructs. Line scan analysis results of fluorescence intensity along the indicated lines are shown on the right. The scale bar is 5 μm

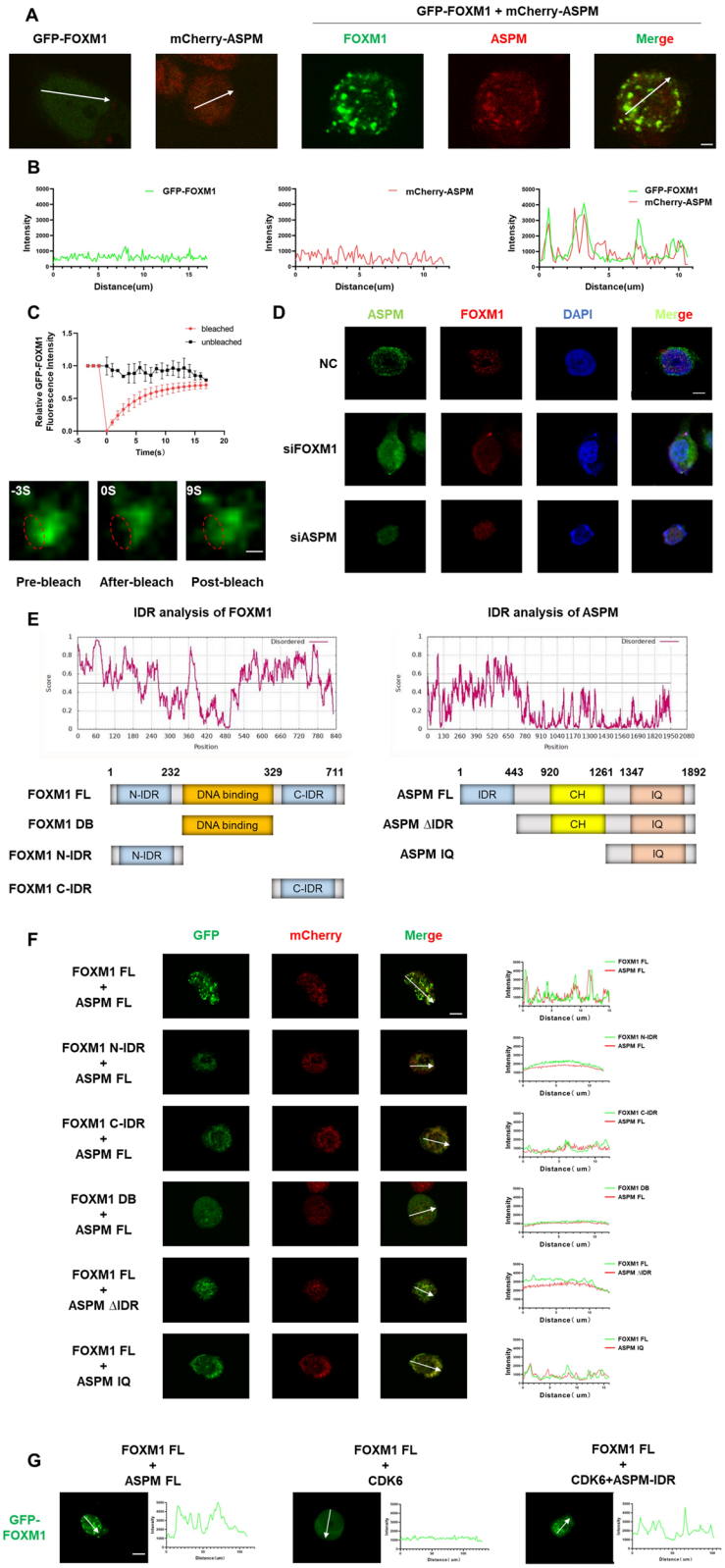


**Fig. 2** (See legend on previous page.)

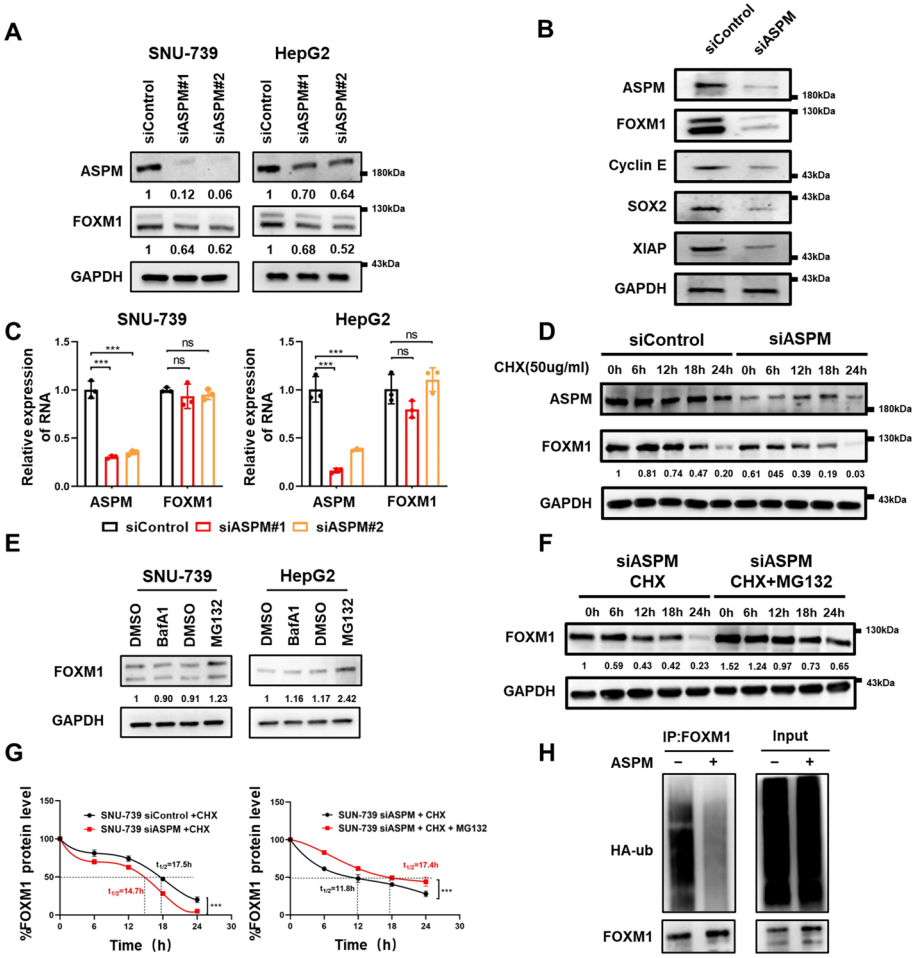


**Fig. 3** ASPM increases the protein stability of FOXM1 in a proteasome-dependent manner. **A** ASPM-targeted siRNAs were transfected into the HCC cell line SNU-739 and HepG2. ASPM silencing effect was tested by Western blot. **B** Western blot was performed to detect the protein levels of the classical downstream genes of FOXM1, including cyclin E1, SOX2, and XIAP in ASPM-knockdown HCC cells. **C** The qRT-PCR assays were performed to detect the mRNA levels of ASPM and FOXM1 in ASPM-knockdown cell lines. The data were presented as the mean ± SD of three independent experiments. The significance was analyzed by the one-way ANOVA. ns, no significance; ***$p < 0.001$. **D** SUN-739 cells were transfected with the indicated siRNAs for 48 h. CHX (50 μg/mL) was then added at 0, 6, 12, 18, and 24 h. Lysates were collected at the indicated time points and immunoblotted with FOXM1, ASPM, and GAPDH antibodies. The average gray density of FOXM1/GAPDH was quantified by software ImageJ and graphed. The experiments were performed in triplicates. **E** Western blot was used to detect the expression of FOXM1 in HCC cells treated with the lysosome inhibitor Bafilomycin A1 (BafA1, 250 nM) and proteasome inhibitor MG132 (20 μM) for 12 h, respectively. GAPDH protein was detected as a loading control. **F** SNU-739 cells were transfected with ASPM siRNAs for 48 h. CHX (50 μg/mL) and MG132 (20 μM) were then added at 0, 6, 12, 18, and 24 h. Lysates were collected at the indicated time points and immunoblotted with the indicated antibodies. The average gray density of FOXM1/GAPDH was quantified by software ImageJ and graphed. The experiments were performed in triplicates. **G** Line chart statistics for Fig. 2 D (left) and 2F (right). Dotted lines indicate half-life of FOXM1. The significance was analyzed by Student's t test. ***$p < 0.001$. **H** ASPM-overexpressing cell lines were established using the expression plasmids. The ubiquitination status and the protein level of FOXM1 were detected by Western blot

Therefore, we used cycloheximide (CHX) to block the biosynthesis of new proteins and to further confirm the effect of ASPM knockdown on the protein level of FOXM1. The half-life of FOXM1 protein was significantly reduced in ASPM-KD cells with the treatment of CHX (Fig. 3D and Fig. 3G left). To further analyze the form of protein

degradation of FOXM1 in ASPM-KD cells, we especially focused on the lysosome and proteasome-mediated protein degradation. Bafilomycin A1 (BafA1) and MG132 are small molecular inhibitors of these two protein-degradation signaling pathways, respectively. It was found that MG132, but not BafA1, elevates protein level of FOXM1 in HCC cells (Fig. 3E), indicating that proteasome-mediated degradation is a dominant regulatory mechanism on the protein level of FOXM1. More importantly, MG132 almost completely eliminates the effect of silencing of ASPM on regulation of the FOXM1 protein level (Fig. 3F and 3G right). And as expected, ubiquitination of FOXM1 was significantly reduced in ASPM-overexpressing HCC cells (Fig. 3H). In summary, these results suggest that ASPM promotes accumulation of FOXM1 by inhibiting its proteasome-mediated degradation.

#### ASPM is required for survival and proliferation of HCC cells in vitro

To investigate the potential role of ASPM in the pathogenesis of human hepatocellular carcinoma, we designed both the loss-of-function and gain-of-function experiments. Firstly, we used two independent siRNAs to knock down ASPM in SNU-739 and HepG2 cells and overexpressed ASPM in MHCC-LM3 cells, respectively. The efficiencies of gene interference and overexpression were confirmed by western blot and qRT-PCR (Additional file 1: Fig. S3A-B). Based on these manipulations, we tested the effect of ASPM on survival and proliferation in HCC cells. As shown in Fig. 4A, the cell viability was significantly reduced with ASPM silencing as determined by CCK-8 assays in HCC

(See figure on next page.)

**Fig. 4** ASPM is essential for proliferation of HCC cells in vitro and in vivo. **A** Cell viability of SNU-739 and HepG2 cells, transfected with siRNAs targeted ASPM (siASPM) or negative control (siControl), was detected by cell counting-8 kit (CCK-8). The data were presented as the mean ± SD of three independent experiments. The significance was analyzed by one-way ANOVA. ***$p < 0.001$. **B** Cell viability of MHCC-LM3 cells, transfected with ASPM-overexpression vector or empty vector (EV), was detected by cell counting-8 kit (CCK-8). The data were presented as the mean ± SD of three independent experiments. The significance was analyzed by Student's t test. ***$p < 0.001$. **C** Plate clone formation assay of SNU-739 and HepG2 cells, transfected with siRNAs targeted ASPM (siASPM) or negative control (siControl), was performed. Clone numbers were measured by ImageJ software. The data were presented as the mean ± SD of three independent experiments. The significance was analyzed by one-way ANOVA. ***$P < 0.001$. **D** Plate clone formation assay of MHCC-LM3 cells, transfected with ASPM-overexpressed vector or empty vector (EV), was performed. Clone numbers were measured by ImageJ software. The data were presented as the mean ± SD of three independent experiments. The significance was analyzed by Student's *t* test. ***$p < 0.001$. **E** Cell proliferation of HCC cells was detected by EdU staining. The scale bar is 50 μm. **F** Statistics of EdU cell proliferation data in Fig. 2E. The cell rate was the ratio between the number of EdU-stained cells and the total cells. The data were presented as the mean ± SD of three independent experiments. The significance was analyzed by one-way ANOVA. *$p < 0.05$.**G** The SNU-739 cells were stably infected with lentivirus expressing the shRNAs targeting ASPM and the control shRNA, respectively. And then, stable clones were injected subcutaneously into the back of 8-week-old nude mice to grow tumors. Subcutaneous tumors were stripped and photographed after injection for 5 weeks. **H** The mice were sacrificed after 5 weeks and tumors were removed to measure the weight. The data were presented as the mean ± SD. The significance was analyzed by one-way ANOVA. **$p < 0.01$, ***$p < 0.001$.**I** The tumor volume was measured and calculated by $V = 0.5 \times Length \times Width^2$. The data were presented as the mean ± SD. The significance was analyzed by one-way ANOVA. **$p < 0.01$, ***$p < 0.001$. **J** Survival curve of mice bearing xenografts was recorded. Mice with a tumor volume greater than 600 $mm^3$ were considered dead.**K** Ki-67 expression of the tumor tissues was detected by IHC and the percentage of positive cells was calculated by ImageJ IHC Profiler. The scale bar is 100 μm. The data were presented as the mean ± SD of three different fields of view at low magnification (× 40). The significance was analyzed by one-way ANOVA. ***$p < 0.001$. **L** The protein levels of ASPM and FOXM1 in subcutaneous tumors were detected by Western blot

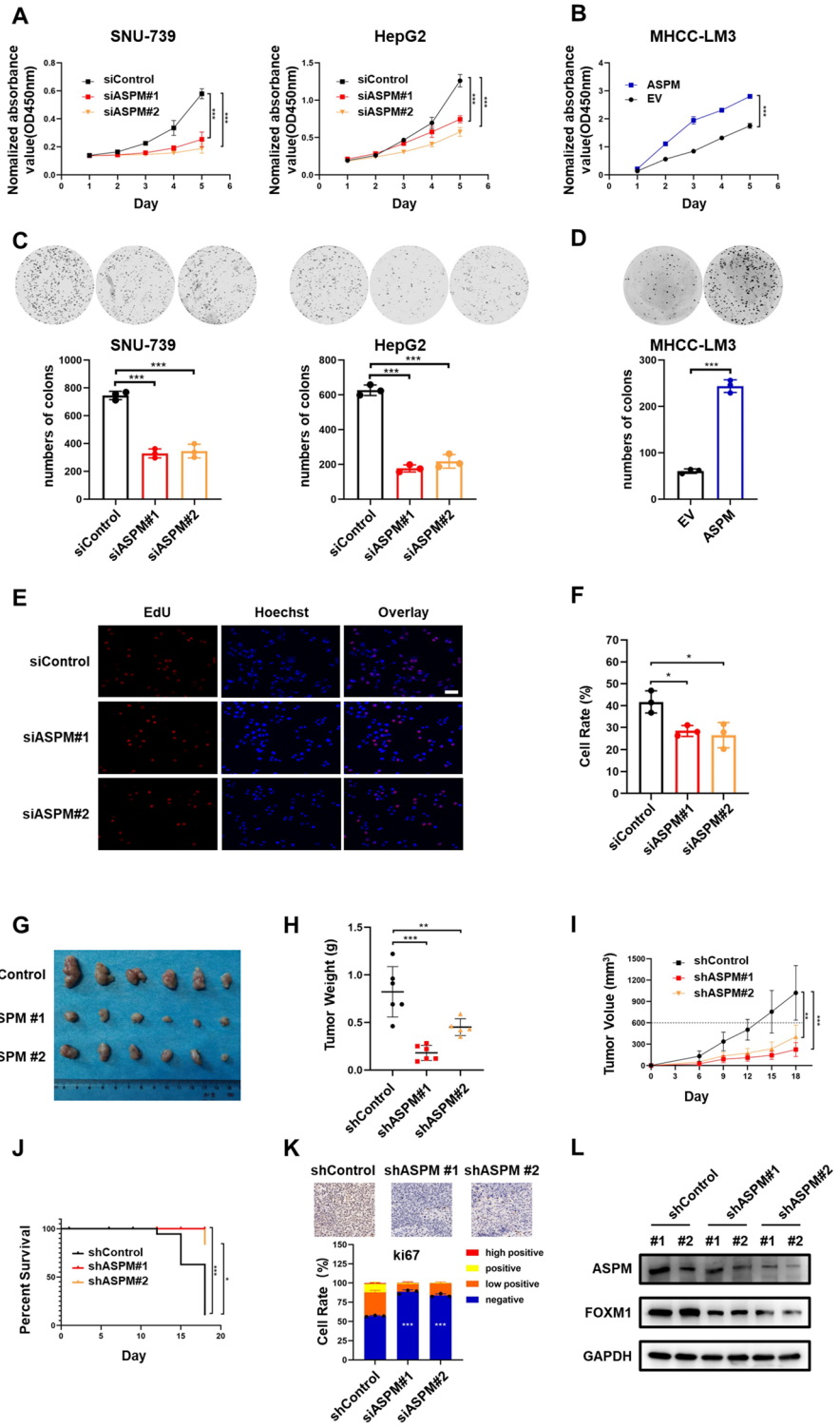


**Fig. 4** (See legend on previous page.)

cells. And the similar results were also observed in the clone formation assays (Fig. 4C). Vice versa, overexpression of ASPM in MHCC-LM3 cells enhanced HCC cell proliferation and clone formation (Fig. 4B, D). Additionally, EdU incorporation assay showed

that silencing of ASPM reduces the proliferation capacity in SNU-739 cells (Fig. 4E, F), whereas overexpression of ASPM enhances the proliferation capacity of MHCC-LM3 cells (Additional file 1: Fig. S3C) in vitro. Collectively, the above data demonstrate that ASPM is required for survival and proliferation of HCC cells in vitro.

#### ASPM is essential for tumor growth in vivo

To investigate the oncogenic roles of ASPM in vivo, we established a nude mouse xenograft model by subcutaneously injecting SNU-739 HCC cells. As shown in F4g. 4G–I, ASPM-deficient tumors had much lower levels in tumor volume, tumor weight, and tumor growth rate compared with the control ones. Moreover, the survival rate of mice with ASPM-deficient xenograft was significantly higher than the control group (Fig. 4J). In addition, with knockdown of ASPM, the signals of Ki-67 staining in tumor tissue sections were significantly reduced (Fig. 4K). Finally, the expression of FOXM1 was almost undetectable in ASPM-deficient tumors (Fig. 4L). All these results suggest that ASPM knockdown suppresses tumor growth and further confirm the essential role of ASPM in advanced progression of HCC in vivo.

#### Re-constitutive expression of FOXM1 weakens ASPM-deficiency induced suppression on HCC growth

To explore the role of FOXM1 in ASPM-involved tumor cell proliferation, we reintroduced exogenous FOXM1 in ASPM-KD cells (Fig. 5A, B). The result of CCK8 assay showed that knockdown of ASPM significantly decreases cancer cell viability; however, this trend of inhibited proliferation is as expected reversed by re-constitutive expression of FOXM1 (Fig. 5C). Similar phenomena were also observed in the clone formation assay and EdU incorporation staining (Fig. 5D, E). Our results demonstrate that re-constitutive expression of FOXM1 weakens ASPM-deficiency induced suppression on HCC growth and emphasizes the critical role of FOXM1 in ASPM-involved tumor growth.

#### ASPM and FOXM1 are coordinately expressed in HCC

According to our above findings that ASPM interacts with FOXM1 and enhances the FOXM1 protein stability by preventing proteasome-mediated degradation, we proposed a proper scenario that ASPM and FOXM1 may be coordinately expressed in HCC. To test this hypothesis, we performed immunohistochemistry (IHC) to investigate the expression of ASPM and FOXM1 in clinical samples of HCC and adjacent normal tissues used in Fig. 1A. The result showed a similar expression pattern of ASPM and FOXM1 in tumor tissues (Fig. 6A,B and Additional file 1: Fig. S4A).

Intriguingly, using the online tools to analyze the expression pattern of ASPM and FOXM1 in serials of independent clinical cohorts, we found that the mRNA levels of ASPM and FOXM1 are frequently co-expressed in almost all types of solid tumors, including hepatocellular carcinoma (Oncomine for Fig. 6C, GEO and TCGA for Fig. 6D and GEPIA for Additional file 1: Fig. S4B). Furthermore, it was observed that mRNA levels of ASPM and FOXM1 have a closely positive correlation in all solid tumor samples from the TCGA database, especially in HCC (Fig. 6E). In addition, the similar expression pattern of ASPM and FOXM1 in protein and mRNA levels were also tested in multiple HCC cell lines (Fig. 6F and Additional file 1: Fig. S4C-D). Taken together, we found that

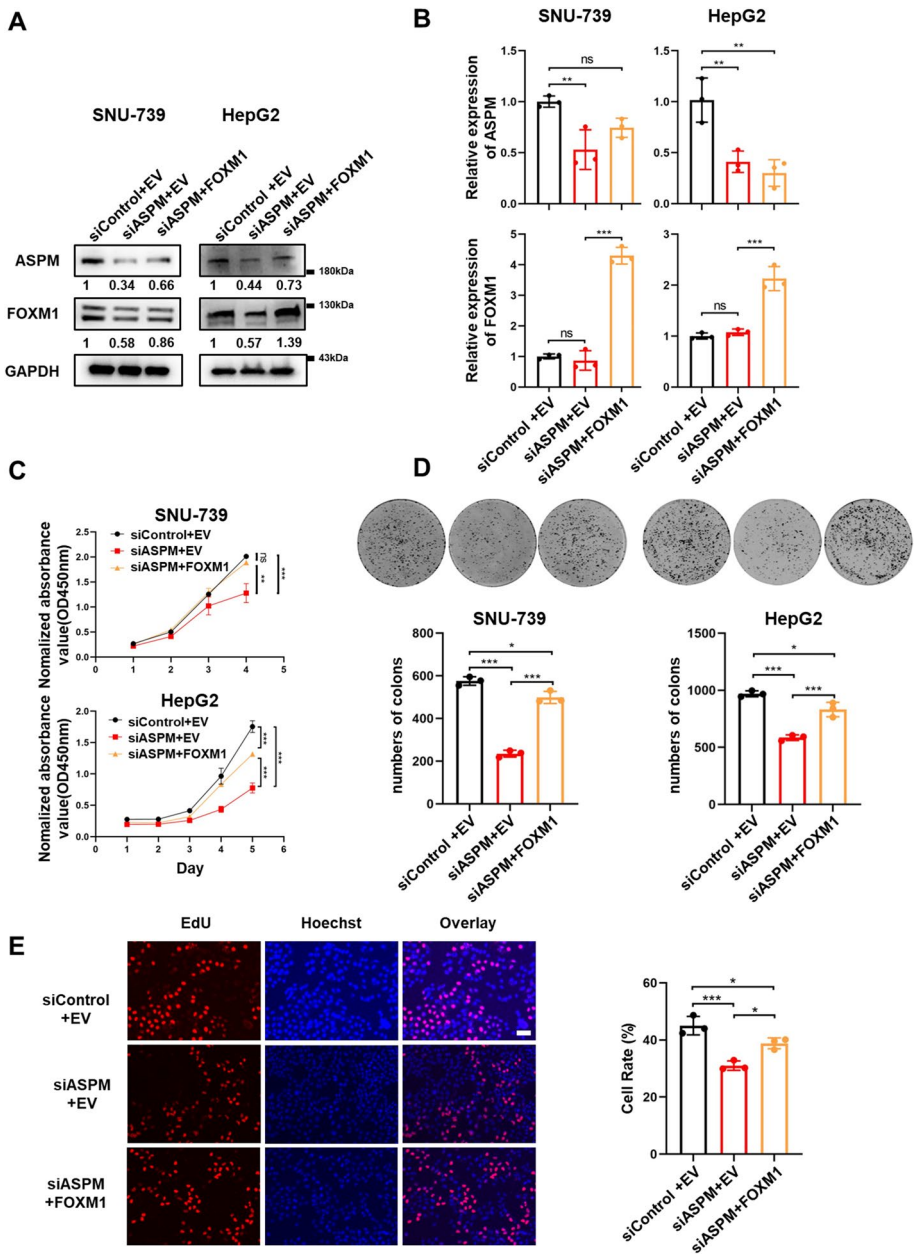


**Fig. 5** FOXM1 is required for ASPM-mediated proliferation in HCC cells. **A** The SNU-739 and HepG2 cells were used to establish ASPM-silencing and FOXM1-overexpressing subclones. The protein levels of ASPM and FOXM1 were detected by Western blot. **B** The mRNA levels of ASPM and FOXM1 were detected by qRT-PCR. The data were presented as the mean ± SD of three independent experiments. The significance was analyzed by one-way ANOVA. ns, no significance; $^{**}P < 0.01$; $^{***}P < 0.001$. **C** Cell viability of indicated cells was detected by cell counting-8 kit (CCK-8). The data were presented as the mean ± SD of three independent experiments. The significance was analyzed by one-way ANOVA. ns, no significance; $^{**}p < 0.01$; $^{***}p < 0.001$. **D** Plate clone formation assay was performed and the number of clones was measured by ImageJ software. The data were presented as the mean ± SD of three independent experiments. The significance was analyzed by one-way ANOVA. $^{*}p < 0.05$, $^{***}p < 0.001$. **E** Cell proliferation was detected by EdU staining. The cell rate was the ratio between the number of EdU-stained cells and the total cells. The data were presented as the mean ± SD of three independent experiments. The significance was analyzed by one-way ANOVA. $^{*}p < 0.05$, $^{***}p < 0.001$. The scale bar is 50 μm

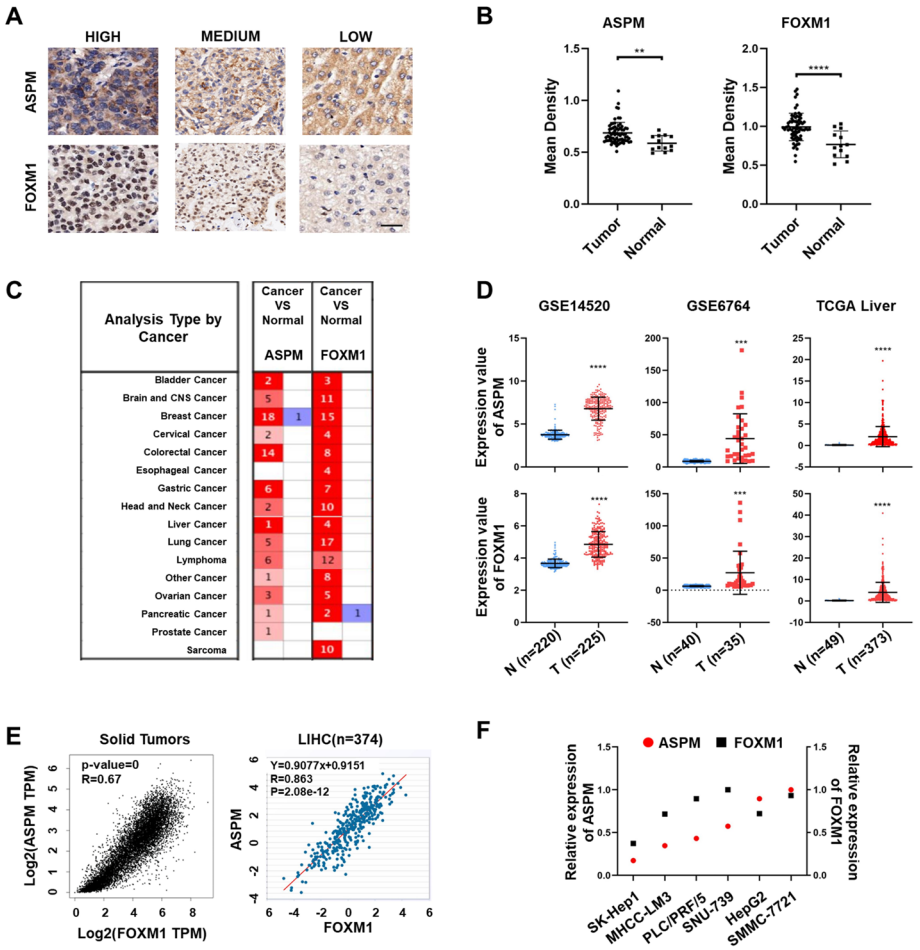


**Fig. 6** Coordinated expression of ASPM and FOXM1 in HCC. **A** Protein levels of FOXM1 and ASPM in HCC samples were analyzed by IHC. The scale bar is 50 μm. **B** Protein levels (H-Score) of FOXM1 and ASPM in tumor and adjacent normal tissues were analyzed by IHC. The significance was analyzed by Student's t test. $^{**}p < 0.01$, $^{****}p < 0.0001$. **C** Analysis of the mRNA levels of ASPM and FOXM1 (cancer vs. normal) in multiple solid cancers from Oncomine database. **D** RNA levels of ASPM and FOXM1 in GEO datasets (GSE6764, GSE14520) and TCGA dataset of HCC. The data were presented as the mean ± SD of different samples. The significance was analyzed by Student's t test. $^{***}p < 0.001$, $^{****}p < 0.0001$. **E** The correlation of FOXM1 and ASPM expression in 31 solid tumors (including ACC, BLCA, BRCA, CESC, CHOL, COAD, ESCA, GBM, HNSC, KICH, KIRC, KIRP, LGG, LIHC, LUAD, LUSC, MESO, OV, PAAD, PCPG, PRAD, READ, SARC, SKCM, STAD, TGCT, THCA, THYM, UCEC, UCS, and UVM) from the TCGA database was analyzed using the GEPIA platform (left), and the correlation of FOXM1 and ASPM expression in LIHC ($n = 374$) TCGA data (right). **F** The correlation between the mRNA levels of ASPM and FOXM1 in six HCC cell lines. mRNA expression was evaluated by qRT-PCR

ASPM and FOXM1 are not only closely correlated in the protein levels, but also have a positive relationship in the mRNA levels in HCC cells.

### Reciprocal regulation of ASPM and FOXM1 forms a double positive feedback loop in HCC cells

According to above findings, we hypothesized that there is a double positive feedback loop between ASPM and FOXM1 in HCC cells. To test this hypothesis, we transiently transfected the exogenous CDS region of ASPM in the HCC cells. Then we designed one pair of qPCR primers, covering the 3'UTR region of ASPM, to detect its endogenous level (Additional file 1: Fig. S5A). The qRT-PCR assay showed that the endogenous ASPM is

upregulated with the expression of exogenous expression of ASPM CDS (Fig. 7A). In addition, we also found that the half-life of total (endogenous and exogenous) FOXM1 is significantly extended with the overexpression of exogenous FOXM1 (Fig. 7B and Additional file 1: Fig. S5B). These results indicated that a double positive feedback loop can promote the expression of ASPM and FOXM1 in HCC cells. Given that the interaction between ASPM and FOXM1 augments FOXM1's transactivation capability in HCC cells, we supposed that FOXM1 might be the upstream regulator of ASPM in HCC cells. As shown in Fig. 7C, D, knockdown of FOXM1 decreases both the protein and the mRNA level of ASPM in SNU-739 and HepG2 cell lines. To further identify the regulatory mechanism of FOXM1 on the expression of ASPM, we searched the public ChIP-seq database and observed a remarkable FOXM1 binding peak in the proximal region of the ASPM genomic locus (Additional file 1: Fig. S5C). In addition, we cloned the canonical promoter region of ASPM (−2000 bp to +500 bp) to validate the FOXM1-medaited transactivation on ASPM. As shown in Fig. 7E, F, overexpression of FOXM1 significantly activates the luciferase activity of the wild-type ASPM promoter. Subsequently, based on the canonical binding motifs of FOXM1 on the target genomic loci, we analyzed the putative binding site of FOXM1 on ASPM promoter and accordingly designed the ChIP-qPCR primers (Fig. 7E). ChIP-qPCR assay showed that FOXM1 significantly interacts with the promoter region of ASPM (−1354 to −1348 bp, −374 to −368 bp and +111 to +117 bp) (Fig. 7G). Taken together, we demonstrated FOXM1 transcriptionally upregulates ASPM and revealed a double positive feedback loop between ASPM and FOXM1 in HCC cells.

#### Co-overexpression of ASPM and FOXM1 is closely related to poor prognosis in HCC

To investigate the clinical significance of an ASPM-FOXM1 feedback loop in progression of HCC, we used the GEPIA tool (http://gepia.cancer-pku.cn/index.html) to mine the bioinformatics data integrated in the TCGA resources according to ASPM and FOXM1 expression. The result showed that patients bearing solid tumors with high levels of ASPM or FOXM1 have lower overall survival rate and disease-free survival rate (Fig. 8A), including HCC (Fig. 8B). To further investigate the effect of co-overexpression of ASPM and FOXM1 on HCC progression, we analyzed the expression status of ASPM and FOXM1. The LIHC patients in TCGA were divided into four groups: (1) FOXM1 $^{High}$ /ASPM $^{High}$, (2) FOXM1 $^{High}$ / ASPM $^{Low}$, (3) FOXM1 $^{Low}$ / ASPM $^{High}$, and (4) FOXM1 $^{Low}$ / ASPM $^{Low}$. The result showed that patients bearing FOXM1 $^{High}$ / ASPM $^{High}$ HCC have much shorter overall survival ($p < 0.01$) than patients whose tumors overexpressed either or neither of ASPM and FOXM1 (Fig. 8C). Moreover, we analyzed the relationship between these molecules and the clinical stages of HCC in the TCGA dataset. With the continuous increase of tumor stage, the expression of ASPM and FOXM1 are gradually increased (Fig. 8D). Collectively, all data here are in accordance with the existence of an ASPM-FOXM1 double positive feedback loop and reveal the prognostic value of the combined utilization of ASPM and FOXM1.

## Discussion

Fork-head box protein M 1 (FOXM1) belongs to the Fox superfamily characterized by a conserved winged helix DNA-binding domain and is a master regulator in the cell cycle signaling network [39]. It has three different isoforms, and among them, FOXM1b (known as FOXM1) is the mostly reported functional transcription factor in multiple

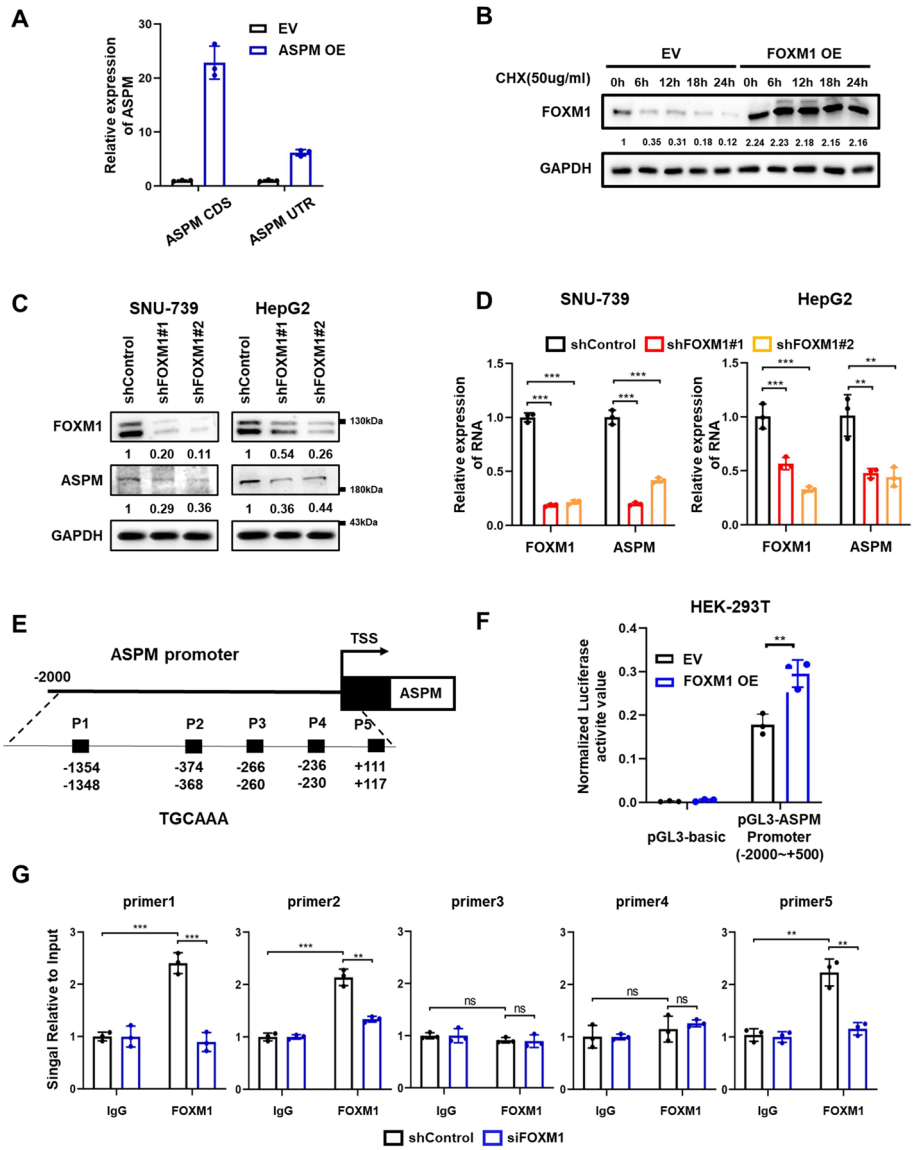


**Fig. 7** FOXM1 transcriptionally activates ASPM in HCC cells. **A** The HCC cell line HepG2 was used to establish ASPM-overexpressing cells by lentivirus infection. Total and endogenous ASPM mRNA levels were detected by qRT-PCR, via the primers at CDS or 3'UTR region in ASPM mRNA (shown in Additional file 1: Fig. S5A). ASPM OE, overexpression of ASPM. EV, empty vector. **B** HepG2 cells were transfected with the indicated plasmids for 48 h. CHX (50 μg/mL) was then added at 0, 6, 12, 18, and 24 h. Lysates were collected at the indicated time points and immunoblotted with the indicated antibodies. FOXM1 OE, overexpression of FOXM1. EV, empty vector. **C** The SNU-739 and HepG2 cells were used to establish FOXM1-knockdown cells by lentivirus mediated shRNA delivery system. The protein levels of FOXM1 and ASPM were detected using Western blot. **D** The qRT-PCR assay was performed to detect the mRNA expression of ASPM and FOXM1 in FOXM1-knockdown cells. The data were presented as the mean ± SD of three independent experiments. The significance was analyzed by one-way ANOVA. $^{**}p < 0.01$, $^{***}p < 0.001$. **E** The binding regions of FOXM1 on ASPM promoter were predicted by bioinformatics. TSS, Transcriptional Start Site. **F** Dual luciferase reporter assay of FOXM1 and ASPM promoter. The data were presented as the mean ± SD of three independent experiments. The significance was analyzed by Student's t test. $^{**}p < 0.01$. FOXM1 OE, overexpression of FOXM1. EV, empty vector. **G** The ChIP-qPCR was used to determine the direct binding of FOXM1 on the promoter region of ASPM in SNU-739 cell lines. Design primers according to Fig. 7E. The data were presented as the mean ± SD of three independent experiments. The significance was analyzed by Student's t test. ns, no significance; $^{**}p < 0.01$; $^{***}p < 0.001$

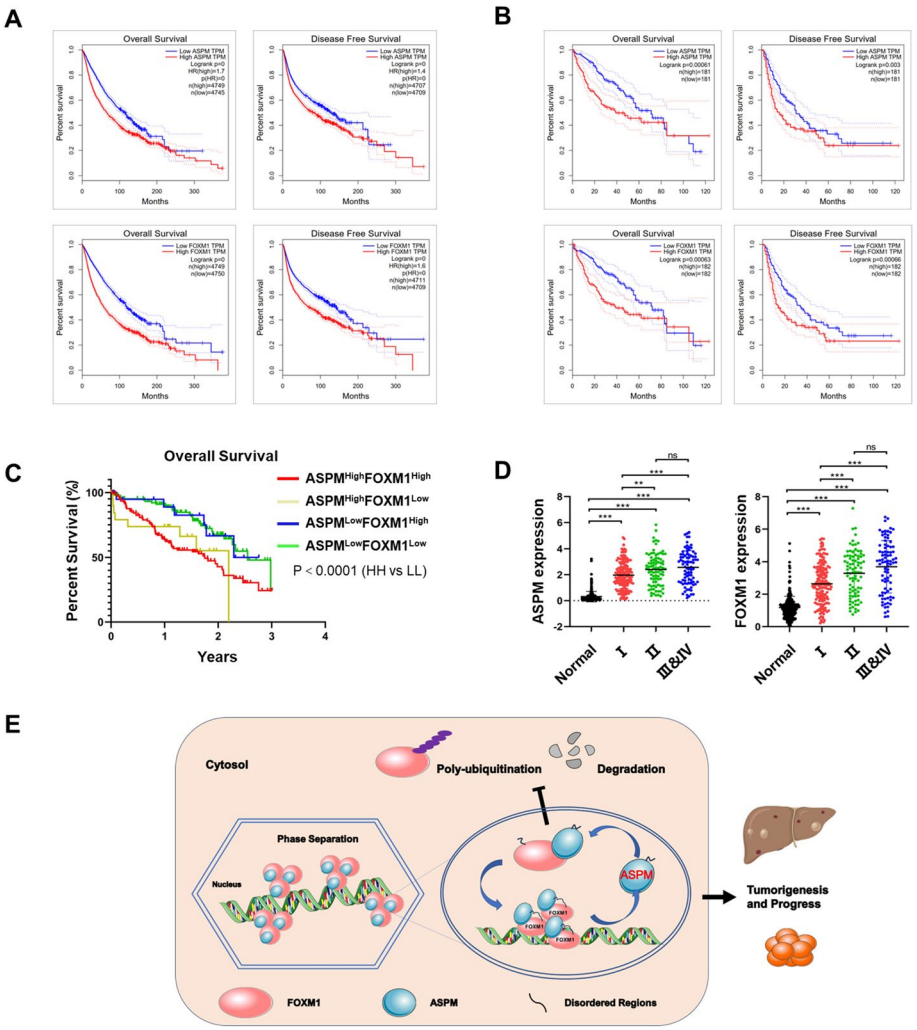


**Fig. 8** The high activation of ASPM-FOXM1 double positive feedback loop is a risk of poor prognosis for HCC patients. **A** Overall survival and disease-free survival rate of 31 solid tumors (including ACC, BLCA, BRCA, CESC, CHOL, COAD, ESCA, GBM, HNSC, KICH, KIRC, KIRP, LGG, LIHC, LUAD, LUSC, MESO, OV, PAAD, PCPG, PRAD, READ, SARC, SKCM, STAD, TGCT, THCA, THYM, UCEC, UCS, and UVM) from TCGA database were analyzed using the GEPIA platform; $n = 9494$. **B** Overall survival and disease-free survival rate of LIHC from TCGA database were analyzed using the GEPIA platform; $n = 364$. **C** Overall survival rate of LIHC from the TCGA dataset was analyzed according to the mRNA levels of ASPM and FOXM1. ASPM High / FOXM1 High ($n = 133$); ASPM High /FOXM1 Low ($n = 21$); ASPM Low /FOXM1 High ($n = 22$); ASPM Low /FOXM1 Low ($n = 118$). **D** The mRNA levels of ASPM and FOXM1 in different stages of HCC. The significance was analyzed by one-way ANOVA. ns, no significance; $^{**}p < 0.01$; $^{***}p < 0.001$. **E** A working model of this study

biological effects [40]. It has been demonstrated that FOXM1 plays a crucial role in mammalian cell division by stimulating expression of genes necessary for cell cycle progression. Several genes that regulate G2/M progression are critically dependent on FOXM1, and cells lacking FOXM1 fail to enter M phase [14]. Although overexpression of FOXM1 is commonly observed in human cancers, there is no high frequency of genetic alterations on the FOXM1 gene, indicating that transcriptional, translational and even trans-locational manners may be involved in the regulation of FOXM1 [31, 41, 42]. For instance, FOXM1 is overexpressed and essential in the progression of Ras-driven HCC [43]. FOXM1 is upregulated by hepatitis B virus X (HBx) through the ERK/

CREB pathway in the progression of HBV-associated HCC [44]. Nuclear translocation of FOXM1 is mediated by CDK4/6 and PLK1 [31, 32]. However, as a transcription factor containing nuclear export signal in coding sequences, why FOXM1 is stuck in the nucleus in HCC is still unknown. In our study, we developed a genome-wide screening assay to find the key molecules, which enhance the entrapment of FOXM1 in the nuclei of HCC cells. Combining subcellular localization information and GSEA results to downstream genes of FOXM1, we could narrow down the gene set to no more than two hundred candidates contained. And it might be a universal method to look for regulators of transcription factors in some subcellular location. This warrants further validation.

Liquid–liquid phase separation (LLPS) is widely observed to directly regulate transcription activity in cancer biology, and the condensed phase usually entraps transcription factors in the nucleus for continuous activation [45, 46]. It was reported that YAP condensates form a transcription hub to maximize target gene expression in anti-PD-1-treated cancer cells [45]. And homotypic and heterotypic mechanisms of LLPS govern NUP98–HOXA9 puncta formation to regulate transcriptional activity and further transformation of hematopoietic cells [46]. Here, we found that a high level of nuclear localized FOXM1 is closely associated with the advanced progression of HCC. Accordingly, we hypothesized that LLPS may be involved in nuclear localization and aberrantly high activation of FOMX1 in HCC cells. Definitely, the functionally associated molecules triggering LLPS should locate in the nuclei of HCC cells. By using a genome-wide screening mentioned above, imaging and biochemical approaches, we demonstrated that FOXM1 interacts with ASPM-iII, a nucleus isoform of abnormal spindle-like microcephaly associated (ASPM) protein and triggers LLPS between FOXM1 and ASPM in the nuclei of HCC cells. LLPS between ASPM and FOMX1 further facilitates FOXM1-driven expression of its downstream oncogenic genes and functionally promotes advanced progression of HCC. According to our knowledge, this study revealed a LLPS involved mechanism promoting FOXM1-driven hepatocellular carcinoma firstly.

Phase-separating biomolecules usually have different roles [5]. Scaffolds, also known as drivers of LLPS, are both necessary and sufficient for phase separation. Clients can selectively partition into scaffold-containing condensates but cannot independently phase separate. In our study, neither over-expressing FOXM1 nor ASPM could form condensates in HCC, separately (Fig. 2A). Meanwhile, knock down of either ASPM or FOXM1 could reduce endogenous condensates obviously (Fig. 2D). It suggests that both ASPM and FOXM1 are not scaffolds (drivers) of LLPS. However, if ASPM and FOXM1 over-expressed in HCC simultaneously, significant condensates form in the nuclei (Fig. 2F). Furthermore, interaction domains (e.g., DNA binding domain of FOXM1) and IDRs are all essential for the LLPS in HCC (Fig. 2E,F). Rescue experiments also confirmed this conclusion (Fig. 2G). Collectively, ASPM and FOXM1 do not function as conventional "drivers" of LLPS individually; however, their IDRs and the interplay between them synergistically facilitate the formation of LLPS condensates in HCC.

Abnormal spindle-like microcephaly associated (ASPM) gene is the human orthologue of the *Drosophila* abnormal spindle (asp) and the most commonly mutated functional gene in autosomal recessive primary microcephaly [47]. Its encoding protein is localized in the centrosome and required for bipolar spindle formation, indicating it plays a critical role in mitotic progression. It was shown that as a mitotic spindle molecule,

the ASPM gene is expressed in proliferating tissues and frequently upregulated in transformed cells [48]. It locates at chromosome 1q31, a region with frequent gain in HCC. Accordingly, it was reported that the aberrant high level of ASPM is closely associated with advanced progression, early tumor recurrence, and even poor prognosis in human HCC [23]. Consequently, an increasing body of studies showed that overexpression of ASPM is a biomarker for poor prognosis in glioblastoma, prostate cancer, gastric cancer, and pancreatic cancer [24–27]. Moreover, the functional experiments demonstrated that ASPM is a potential target in multiple cancers. Nevertheless, the understanding on ASPM-driven oncogenic mechanism remains elusive. The previous explanation is that ASPM affect the activation of β-catenin-mediated oncogenic transcriptional signaling pathways through a molecular interaction in the cytoplasm. It was identified that ASPM in the cytoplasm interacts with Dvl1/2/3 proteins, which relieve the binding of β-catenin to the inhibitor of β-catenin and T-cell factor (ICAT), leading to nuclear translocation of β-catenin and its oncogenic transactivation [24–26, 29]. In the present study, we identified nucleus-located ASPM, also known as ASPM-iII, interacts with the DNA binding domain (DBD) of FOXM1 through its intrinsically ordered regions (IQ domains) and drives LLPS of FOXM1 in the nucleus of HCC cells via their intrinsically disordered regions (IDRs). Although the nucleus-located ASPM is not documented in the Uniport database, we predicted its reliable structure using AlphaFold2, particularly for its C-terminal ordered regions (Additional file 1: Fig. S2C). Furthermore, although ASPM is not a DNA-binding protein, our ChIP-sequencing data using ASPM-specific antibody showed that it can occupy on the genomic loci. More importantly, the respective binding peaks of ASPM and FOXM1 in the annotated genes are highly overlapped, indicating ASPM may facilitate FOXM1-driven oncogenic signaling. In addition, data from the loss of function experiments in vitro and in vivo further confirmed the important role of ASPM in tumorigenesis of HCC. Mechanistically, ASPM interacts and triggers LLPS with FOXM1 in the cellular nuclei and consequently enhances the stability FOXM1 protein by preventing proteasome-mediated degradation, which augments the FOXM1-driven oncogenic transactivation capability in HCC cells. Recently, it has been proposed that E3 ligase-based proteolysis-targeting chimeras (PROTAC) could be a potential strategy to promote degradation of the FOXM1 oncoprotein [49]. However, one issue should be given sufficient attention, in which the molecular interaction between ASPM and FOXM1 is likely to lead to FOXM1's resistance to ubiquitination modification and consequent proteasome-mediated degradation. This indicates that disruption of the molecular interaction between ASPM and FOXM1 could be a key step to inhibit FOXM1's carcinogenic effects. Therefore, our findings here not only expanded the underlying mechanisms of ASPM-involved oncogenic effects in HCC, but also proposed a rational therapeutic strategy in patients with both high levels of ASPM and FOXM1. The investigation of whether the inhibition of ASPM and FOXM1 interaction holds potential benefits for HCC patients necessitates further exploration.

Clinically, although ASPM and FOXM1 have been reported to be indicators for poor prognosis in HCC, respectively, we demonstrated that co-overexpression of ASPM and FOXM1 could be a more potential biomarker to poor prognosis in HCC. Collectively, in the present study, we identified a physical interaction between ASPM and FOXM1, which reinforces FOXM1-mediated pro-cancer transcriptional regulation in HCC cells.

Mechanistically, ASPM forms condensed phase with FOXM1 in the nuclei, thereby protecting FOXM1 from the proteasome-dependent degradation in HCC cells. More importantly, ASPM is identified as a direct downstream gene transcriptionally regulated by FOXM1 in HCC cells. And the high frequency of coordinately expression of ASPM and FOXM1 is closely associated with poor prognosis in HCC. In summary, our study demonstrates that reciprocal regulation of ASPM and FOXM1 amplifies the oncogenic progression and an ASPM-FOXM1 double positive feedback regulatory loop could be a potential biomarker and therapeutic target in human hepatocellular carcinoma.

## Conclusions

Our study reveals that liquid–liquid phase separation (LLPS) between ASPM and FOXM1 entraps FOXM1 in the nuclei of HCC cells and stabilize FOXM1 proteins in HCC. In addition, ASPM is transcriptional activated by FOXM1 in HCC. Collectively, our findings underscore the significance of an ASPM-FOXM1 double positive feedback loop as a potential biomarker and therapeutic target for HCC.

## Methods

### Patients and specimens

This study was approved by the Medical Ethics Committee of the First Affiliated Hospital of the Air Force Medical University (approval number: XJYYLL-2015625). The supplier of samples completed the informed consent of all patients in the process of data collection. The clinicopathological characteristics of the HCC patients are listed in Additional file 1: Table S1. Tissue microarrays were prepared as previously reported [50].

### Immunohistochemistry (IHC) staining and analysis

Tissue microarrays were deparaffinized with xylene (3 × 15 min) and rehydrated with serial dilutions of ethanol (2 × 100%, 1 × 85%, and 1 × 75%, 5 min each) followed by rinsing in $ddH_2O$. Heat-mediated antigen retrieval was performed by microwaving with EDTA pH 9.0. The sections were cooled on a decolorization shaker in PBS (3 × 5 min), immersed in 3% hydrogen peroxide, incubated at room temperature in darkness for 25 min, washed three times with PBS, and incubated for 30 min in blocking solution (3% BSA). The primary antibodies (anti-FOXM1, Santa Cruz Biotechnology, sc-376471, 1:50) and anti-ASPM (Proteintech, 26,223–1-AP, 1:100) were diluted with PBS and incubated with sections for 1 h at 37 °C or overnight at 4 °C. The sections were washed three times for 5 min (3 × 5 min) with 1 × PBS on a shaker and then incubated with secondary antibody (HRP labeled) for 500 min at 37 °C. The sections were then washed 3 × 5 min with PBS and stained with the Immunohistochemical kit DAB chromogenic agent (Servicebio, G1211). The color development time was controlled under the microscope. The sections were counterstained with hematoxylin stain solution for approximately 3 min. Finally, tissues were dehydrated and mounted in Eukitt medium.

Images were captured with a light microscope. Histochemistry score (H-score) of nucleus and total cells were analyzed by AIPATHWELL software (developed by Wuhan Servicebio Technology Co.). The comparation and correlation of protein expression was analyzed using GraphPad Prism (Version 8; La Jolla, CA, USA).

### Cell lines and cell culture conditions

Human hepatocellular carcinoma cell line MHCC-LM3 and human hepatocellular carcinoma cell line SNU-739 were cultured in PRMI Medium 1640 (GIBCO BRL, Grand Island, NY, USA) with 10% fetal bovine serum (GIBCO BRL), penicillin (100 mg/ml), and streptomycin (100 mg/ml). Human hepatocellular carcinoma cell line HepG2 and human embryonic renal epithelial cell line HEK293T were cultured in Dulbecco's modified Eagle's medium (GIBCO BRL) with 10% fetal bovine serum (GIBCO BRL), penicillin (100 mg/ml), and streptomycin (100 mg/ml). Human hepatocellular carcinoma cell lines SNU-739, HepG2, and MHCC-LM3 were obtained from the Type Culture Collection of the Chinese Academy of Sciences. Human embryonic renal epithelial cell line HEK293T was purchased from ATCC (Manassas, VA, USA). All cells are tested quarterly to make sure they are mycoplasma free.

### DNA construction

The human FOXM1 and ASPM shRNAs were constructed by ligation of oligonucleotide sequences targeting human FOXM1 and ASPM into the Age l and EcoR l digested pLKO.1-TRC cloning vector (Addgene, Cambridge, MA, USA; 10,878). The pCDH-FOXM1 plasmid was constructed via insertion of a PCR-amplified human FOXM1 cDNA into a pCDH vector digested with BamH l and EcoR l. The pcDNA3.1-ASPM-mCherry plasmid was constructed via insertion of a PCR-amplified human ASPM cDNA into a pcDNA3.1-mCherry vector digested with Nhe l and Kpn l, and the corresponding mCherry fusion genes including ZFP91, CDC27, MORC3, PHF20L1, and CDK6 were also constructed using the similar strategy. The pcDNA3.1-FOXM1-GFP plasmid was constructed via insertion of a PCR-amplified human FOXM1 cDNA into a pcDNA3.1-GFP vector digested with Hind III and BamH l. The pCMV-ASPM-3 × Flag plasmid was purchased from Genechem (Shanghai, China). For siRNA treatments, siASPM#1, siASPM#2, and siControl were purchased from GenePharma (Shanghai, China). The sequences of shRNAs and siRNAs are listed in Additional file 1: Table S5.

### Cell line treatments

To inhibit lysosome function, cells were cultured with 250 nM BafA1 (Selleck, S1413) for 12 h. To inhibit proteasome function, cells were cultured in 20 μM of MG132 (GLPBIO, GC10383) for 12 h. To inhibit nascent protein synthesis, cells were cultured with 50 ug/ml Cycloheximide (CHX, Selleck, S7418) for a specific time.

### Western blot

Cells were collected and washed with phosphate buffer saline (PBS) three times, and then harvested using RIPA Lysis Buffer. Protein in the cell lysate was resolved on 8–15% SDS polyacrylamide gel and transferred to a nitrocellulose membrane. Before incubation with primary antibodies, the membrane was blocked with 5% nonfat milk. Membranes were incubated with the corresponding antibodies overnight at 4 °C. After incubation with peroxidase-conjugated secondary antibodies for an hour at room temperature, the signals were visualized using ECL chemiluminescent

reagents by Tanon 5500 (Tanonn Science & Technology; Shanghai; China). The following antibodies and dilutions were used: anti-FOXM1 (1:1000; Santa Cruz Biotechnology sc-376471), anti-ASPM (1:500; proteintech; 26,223–1-AP), anti-GAPDH (1:1000; proteintech; 10,494–1-AP), anti-Histone H3 (1:1000; Cell Signaling Technology; 9715), anti-SOX2 (1:1000; EPITOMICS; 2683–1), anti-cyclinE1 (1:1000; abcam; ab3927), anti-XIAP (1:1000; abcam; ab21278), anti-Integrin α5 (1:1000; Cell Signaling Technology; 98,204), anti-LaminA/C (1:1000, proteintech, 10,298–1-AP).

#### Quantitative RT-PCR

RNA isolation and quantitative real-time PCR were performed as previous described. Briefly, $5 \times 10^6$ cells were harvested for purification of total RNA using TRIzol Reagent (Invitrogen), and 1 μg of total RNA of each sample was reversed to cDNA by PrimeScript RT Master Mix (TaKaRa, Tokyo, Japan). For detecting the mRNA level of specific genes, the diluted cDNA of each sample was used as a template to perform quantitative PCR and the amplifications were done using SYBR-green PCR MasterMix (TaKaRa). RT-PCR assays were performed three times and the fold changes of genes were obtained after normalizing to GAPDH using the comparative Ct method (fold change $= 2^{-\Delta\Delta Ct}$). Primers used for quantitative RT-PCR are listed in Additional file 1: Table S6.

#### ChIP sequencing

ChIP, sequencing library preparation, and data analysis were conducted by LC-Bio (Hangzhou, Zhejiang, China). Genomic DNA degradation and contamination were monitored on 1% agarose gels. DNA purity was checked using the NanoPhotometer® spectrophotometer (IMPLEN, CA, USA). The DNA concentration was measured using a Qubit® DNA Assay Kit in a Qubit® 2.0 Fluorometer (Life Technologies, CA, USA). A total amount of 50 ng DNA per sample was used as input material for the ChIP sample preparations. The Chip-Seq library construction mainly includes the steps of cell crosslinking, cell lysis, protein co-immunoprecipitation, extraction of co-precipitated complex DNA, and construction of DNA next-generation sequencing library. Sequencing libraries were generated using NEBNext® Ultra™ DNA Library Prep Kit for Illumina® (NEB, USA) following the manufacturer's recommendations and index codes were added to attribute sequences to each sample. Briefly, Chip DNA was end-blunted and added with an "A" base so the adaptors from Illumina with a "T" can ligate on the ends. Then we used magnetic beads to recover the target size fragments and performed PCR amplification to obtain the library to be sequenced. The constructed library was checked for quality by agarose electrophoresis. Libraries were quantified using Qubit 2.0 to determine if the library concentration was suitable for use on the machine. After the library quality inspection was qualified, different libraries were sequenced on the Illumina sequencer according to the requirements of effective concentration and target data volume. The clustering of the index-coded samples was performed on a cBot Cluster Generation System using a HiSeq Rapid Duo cBot Sample Loading Kit (Illumina) according to the manufacturer's instructions. MACS2 (v2.1.1) was used to call peak, giving a robust and high-resolution ChIP-Seq peak predictions. Peaks were annotated related genes using Homer (v4.10). ChIPseeker (v1.5.1) was used to depict the reads distribution on chromosomes. Homer (v4.10) was used to search motif and analyze transcription factors.

#### Fluorescence recovery after photobleaching (FRAP)

For FRAP experiments in living cells, an area of FOXM1 puncta were bleached for 500 ms using 10% laser power (405 nm laser line) and images were collected every 2 s post-bleaching using Olympus FV3000 invert confocal. Fluorescence intensities were quantified using the Olympus Cellsens software. GFP fluorescence signal was collected over time and photobleaching was performed after three fluorescence signals were collected. The droplet was photobleached in three regions ROIs that were defined for these experiments. ROI-1 was the indicated circular region in the droplet, and ROI-2 was a similarly sized circular region in the same droplet but in an area that was not photobleached. ROI-3 was defined as background and drawn outside the droplet and its signal was subtracted from both ROI-1 and ROI-2. Fluorescence intensity was measured using Cellsens and plotted using Prism software. Each data point is representative of the mean and standard deviation of fluorescence intensities in three unbleached (control) or three bleached (experimental) granules. And the prebleached fluorescence intensity was normalized to 1.

#### Subcellular fractionation

The subcellular fractionation was performed as described previously using a Qproteome Cell Compartment (QIAGEN, 1,073,571). Briefly, lysis Buffer was added to cells and selectively disrupted the plasma membrane without solubilizing it, resulting in the isolation of cytosolic proteins. Plasma membranes and compartmentalized organelles, such as nuclei, mitochondria, and the endoplasmic reticulum (ER), remained intact and were pelleted by centrifugation. Next, the pellet from the previous step was resuspended in Extraction Buffer CE2, which solubilizes the plasma membrane, as well as all organelle membranes except the nuclear membrane. After solubilization, the sample was centrifuged. The supernatant contains membrane proteins and proteins from the lumen of organelles (e.g., the ER and mitochondria). The pellet consists of nuclei. In the next step nuclei were solubilized using Extraction Buffer CE3 in which all soluble and most membrane-bound nuclear proteins are extracted. Addition of Benzonase® Nuclease allows the release of proteins tightly bound to nucleic acids (e.g., histones). After another centrifugation, Extraction Buffer CE4 was used to solubilize all residual — mainly cytoskeletal — proteins in the pellet.

#### Dual luciferase reporter assay

Cells were co-transfected with pGL3-ASPM-promoter, pRL-TK, and pCMV-FOXM1 / GFP using Lipofectamine 2000 (Invitrogen). Cell extracts were prepared and luciferase activity was measured using the Dual Luciferase Reporter Assay System (Promega, Madison, WI, USA). The relative firefly luciferase activity was normalized with its respective Renilla luciferase activity.

#### Chromatin immunoprecipitation assay

The chromatin immunoprecipitation analysis was performed as described previously using a SimpleChIP Enzymatic Chromatin IP Kit (Cell Signaling Technology, 9003). Hepatocellular carcinoma cell line SNU-739 or HepG2 were infected with siControl or siRNAs. A total of $1.2 \times 10^7$ cells were crosslinked with 1% formaldehyde solution for

15 min at room temperature. The crosslink reaction was then stopped by addition of 10% glycine and lysed in 1 ml lysis buffer on ice. Lysates was harvested and sonicated into DNA fragments with 150–900 bp using the Micrococcal nuclease and Scientz-1500F Ultrasonic disperser (Ning Bo, China). Sonicated samples were spun down and subjected to overnight immunoprecipitation with IgG or FOXM1 antibody (Santa Cruz Biotechnology). After the proteins and RNA are removed by Protease K and RNase A, the chromatin pulled-down by antibodies is purified. The enrichment of ASPM is detected by qPCR amplification. Primers for qPCR amplification are listed in Additional file 1: Table S7.

#### EdU cell proliferation

The EdU cell proliferation analysis was performed as described previously using a Meilun EdU Cell Proliferation Kit with Alexa Fluor 555 (mellunbio, MA0425). An appropriate number of cells were inoculated in a 96-well plate and cultured overnight and incubated with 10 μM EdU working solution for 2–3 h. After EdU labeling was completed, the culture medium was removed and 1 ml 4% paraformaldehyde was added to fix at room temperature for 15 min. Cells were washed 3 times with washing solution for 3–5 min each time. After being added permeabilization solution and incubated for 10–15 min, the cells were washed three times again. And then, cells were incubated with 200 μl Click reaction solution for 30 min in the dark to label cells with bright red fluorescence. And the nuclei were stained with Hoechst33342.

#### Immunofluorescence and confocal microscopy

SNU-739 cells were seeded on chamber slide and subsequently fixed with 4% PFA for 15 min, permeabilized with Triton-X 100 for 20 min at 37℃ and blocked with 5% BSA in PBS. Then cells were incubated with FOXM1 antibody (Santa Cruz Biotechnology; sc-376471; 1:200) and ASPM antibody (proteintech; 26,223–1-AP; 1:200) overnight at 4 °C. And then cells were stained with Alexa Flour 555 and Alexa Fluor 488 (1:1000, Life Technologie). The nuclei were stained with DAPI. Images were visualized using a Nikon confocal microscope.

#### Cell viability assay

Cell viability was analyzed using Cell Counting Kit-8. Cells were pre-seeded in 96-well plates with the number of $1 \times 10^3$. The cell culture medium was discarded and replaced with culture medium containing 0.5 μg/μl Cell Counting Kit-8 (0.5 mg/ml) reagent and cells were incubated at 37℃. After 0.5–4 h, the absorbance of the culture medium was detected using a Bio-RAD (Hercules, CA, USA) Microplate Reader with a wavelength of 450 nm.

#### Colony formation assay

Long-term cell survival was monitored by the colony formation assay. In brief, 1000 cells were seeded into 6-well plates and allowed to grow for 2 weeks. Cells were fixed with 4% paraformaldehyde for 15 min and stained by 0.5% (w/v) crystal violet (Sigma Aldrich). Colons in the plate were scanned using Odyssey Scanner (LI-COR, Lincoln, NE, USA) and the number of colons was quantified by ImageJ software.

### Protein stability assay

The cycloheximide (CHX)-based assay was performed as previously described to evaluate protein turnover in cells. To determine the half-life of FOXM1 protein, 50 μg/ml CHX was added to the cell culture medium and cells were harvested at the indicated time points. Then, cells were lysed with RIPA and protein levels of FOXM1, ASPM, and GAPDH were performed with western blot. To block the proteasome-mediated protein degradation, cells were incubated with 20 μM MG132 and 50 μg/ml CHX simultaneously and harvest cells at the indicated time points. Finally, protein levels of FOXM1 were quantified by gray scale scanning using the ImageJ software.

### Immunoprecipitation assay

The number of $1 \times 10^7$ HepG2 cells were washed with pre-chilled phosphate-buffered saline (PBS) and lysed with NP-40 containing protease inhibitors. Cell lysates were incubated on ice for 10 min and centrifugated with 12,000 rpm for 15 min. The supernatant was then transferred to a new centrifuge tube. Antibodies were added and incubated at 4 °C for 3 h with rotation for immunoprecipitation. Finally, magnetic beads conjugated protein G (Thermo Fisher) were incubated overnight at 4 °C to capture immune-complexes. The immuno-complexes were subjected to western blot assay after washing the beads.

### Animal studies

To generate mouse subcutaneous tumors, male 8-week-old BALB/c nude mice were implanted subcutaneously in the flank of back with $1 \times 10^7$ HCC cells. The mice were housed in 3–5 per cage under specific pathogen-free conditions in a 12-h light/dark cycle with food and water ad libitum. The experiments were approved by the Institutional Animal Experiment Administration Committee of the Fourth Military Medical University (IACUC-20171005). The volume of the tumor was measured every 3 days after the tumor was successfully loaded. The mice were sacrificed after 5 weeks and in vivo solid tumors were dissected and weighed. Tumor volume was determined using the formula $0.5 \times L \times W^2$, where L is the longest diameter and W is the shortest diameter. Tumors were removed into 4% polyformaldehyde solution for fixing tissues. Our study examined male mice because male mice exhibited less variability in phenotype.

### Molecular docking

The protein structures of ASPM, ZFP91, CDC27, MORC3, and PHF20L1 were predicted by Alphafold2 as previously reported [37]. The 3D structure of the FOXM1 (PDB ID: 3G73) was downloaded from RCSB Protein Data Bank (https://www.pdbus.org/). Protein–protein docking between each of the five molecules and FOXM1 was simulated online by ClusPro server (https://cluspro.org) [51]. Non-covalent interactions between proteins were identified by Protein Ligand Interaction Profiler (https://plip-tool.biotec.tu-dresden.de/) [52]. Molecular graphics were generated using PyMOL as previously described [53].

### Public database

Subcellular localization information was downloaded from UniProt database (https://www.uniprot.org/). The expression of FOXM1 and ASPM in different cancer tissues and normal tissues were analyzed using Oncomine database (https://www.oncomine.org/). The mRNA levels of FOXM1 and ASPM in hepatocellular were obtained from Gene Expression Omnibus (GEO, https://www.ncbi.nlm.nih.gov/geo/) and normalized using GEO2R. Correlation analysis and survival analysis of FOXM1 and ASPM from 31 TCGA solid tumors was done using Gene Expression Profiling Interactive Analysis (GEPIA, http://gepia.cancer-pku.cn). RNA-seq data of Cdk4/6 and Plk1 in hepatocellular carcinoma were from The Cancer Genome Atlas Liver Hepatocellular Carcinoma (TCGA-LIHC) database (https://portal.gdc.cancer.gov/). The raw count matrix of RNA-seq was converted into transcripts per kilo million (TPKM). The correlation data of FOXM1 and ASPM from TCGA were obtained using cBioportal for cancer genomics (http://www.cbioportal.org). The FOXM1-related protein was analyzed using STRING database (https://string-db.org/). The intrinsic unstructured proteins were analyzed from an IUPred2A-based online tool (https://www.novopro.cn/tools/disordered.html) and ANCHOR Database (https://iupred.elte.hu/). The public ChIP-seq data was obtained from ENCODE database (https://www.encodeproject.org/).

### Gene set enrichment analysis (GSEA)

A novel gene subset for GSEA was defined according to a widely accepted FOXM1 downstream gene list previously [35]. For each nucleus-located gene, 374 TCGA-LIHC samples were divided into high and low groups according to the median expression of this gene. Then, differential expression gene analysis between the high and low groups were performed by "DEseq2" R package, and GSEA assays were done by the "clusterProfiler" R package. Normalized enrichment score (NES) and $p$ value of all the intranuclear genes were used for further analysis.

### Manders' colocalization coefficients

Fluorescence co localization analysis characterized by Manders' Colocalization Coefficients (MCC) using the ImageJ plugin Coloc 2. M1 and M2 represent the portion of a protein colocated with another protein, accounting for the proportion of the total amount of this protein. ROIs were set manually around the cytoplasm of the cells, excluding the background from the analysis. Results from three independent experiments were pooled.

### Statistics

The in vitro experiments were repeated at least three times unless stated otherwise. As indicated in the figure legends, all quantitative data were presented as the mean ± SD of three biologically independent experiments or samples. Statistical analysis was performed using GraphPad Prism 8 (GraphPad, San Diego, USA). Comparisons between two groups were done by two-tailed unpaired or paired Student's $t$ test. Comparisons among three or more groups were done with ANOVA followed

by Tukey's multiple comparison post-test. The correlation of protein expression was analyzed by linear regression analysis. $p < 0.05$ was considered as significant ($^{*}p < 0.05$, $^{**}p < 0.01$, $^{***}p < 0.001$).

## Supplementary Information

The online version contains supplementary material available at https://doi.org/10.1186/s13059-025-03526-5.

Additional file 1: Fig. S1. A genome-wide screen identifies ASPM involved in phase separation of FOXM1 in nucleus and promoting transcription activity of FOXM1 in HCC. Related to Figure 1. Fig. S2. FOXM1 interacts and forms dynamic condensates with ASPM. Related to Figure 2. Fig. S3. Decreased HCC cells proliferation was caused by ASPM silencing. Related to Figure 4. Fig. S4. ASPM and FOXM1 have positive correlation in multiple cancers. Related to Figure 6. Fig. S5. FOXM1 transcriptionally activates ASPM in HCC cells. Related to Figure 7. Table S1. Clinicopathological characteristics of 62 HCC patients. Table S2. Numbers of different intermolecular forces between indicated proteins and FOXM1. Data were from Protein-Ligand Interaction Profiler. Table S3. Docking analysis of ASPM and FOXM1 by Protein-Ligand Interaction Profiler. Table S4. Manders' Colocalization Coefficients (MCC). Table S5. Sequences of shRNA. Table S6. Primers used for qPCR. Table S7. Primers used for ChIP-qPCR.

Additional file 2: Uncropped western blot images.pdf.

Additional file 3: Review history.

**Acknowledgements**

Our acknowledgement to Dr. Xiao Zhang, Dr. Bo Yan, and Dr. Chenjun Guo for advising and teaching to experimental design and operation, and Xiaofang Zhang for her help in molecular cloning and plasmid construction. We also appreciated the scientific and technical services provided by the Experimental Surgery Department of Xijing Hospital, especially the experimental animal feeding services. Finally, the support of confocal microscope and fluorescence microscope from the Department of Biochemistry and Molecular Biology and the Department of Immunology gave us a lot of help.

**Review history**

The review history is available as Additional file 3.

**Peer review information**

Gian Gaetano Tartaglia and Andrew Cosgrove were the primary editors of this article and managed its editorial process and peer review in collaboration with the rest of the editorial team.

**Authors' contributions**

XZ, JL, and RZ designed the study, obtained the funding, and supervised all the work. XJ was the main responsible for most of the experiments, with the help and supervision of JL, KW, and JS. HY provided great help for immunofluorescence, IP, and ChIP assays. YJ, NW, and XD contributed to the in vivo experiments in nude mice. YL and LL performed the bioinformatic analysis. PG helps the phase separation work. XZ and XJ wrote the first draft of the manuscript that was revised critically for important intellectual content by JL and RZ and approved by all the authors. All authors read and approved the final manuscript.

**Funding**

This work was supported by grants from the National Key Research and Development Program of China (2023YFC2308101 to R.Z.); the National Natural Science Foundation of China (82173046 and 82472702 to R.Z.; 82172781 to J.L; 82173162 to X.Z; 81802808 to J.S; 31801128 to H.Y and 82403237 to K.W.); Fund for Scientific and Technological Innovation Team of Shaanxi Innovation Capability Support Plan (2022TD-47 to R.Z.); Shaanxi Province Funds for Distinguished Young youths (2023-JC-JQ-66 to R.Z.); Shaanxi Province Key Industrial Innovation Chain Project (2024SF ZDCYL-04–04 to R.Z.); Development funding of the Fourth Military Medical University (2023JC001 to R.Z. and P.G.); Medical Advancement Program of the Fourth Military Medical University (2021JSTS34 to X.Z.); and the Fund of State Key Laboratory of Holistic Integrative Management of Gastrointestinal Cancers (CBSKL2022ZZ47 to X.Z.).

**Data availability**

Source data are provided with this paper. ChIP-seq raw data and processed expression matrix are uploaded to GEO DataSets under accession code GSE218100. The microscopy data and uncropped western blot images are deposited in Figshare database (https://doi.org/10.6084/m9.figshare.28390316.v1). All other data analyzed or generated in this study are provided along with the article. The data of the human tumor dataset can be accessed through GEO under accession numbers GSE14520 [54] and GSE6764 [55]. The packaged benchmark workflow with detailed documentation and all benchmark results in simulated and real data are available in the GitHub repository (https://github.com/ykliu2025/liu_250208) [56] and Zenodo (https://doi.org/10.5281/zenodo.14835716) [57]. The source code is released under CC BY 4.0 license.

## Declarations

**Ethics approval and consent to participate**

Informed consent was obtained for donation of hepatocellular carcinoma and adjacent tissue samples according to the Declaration of Helsinki and after approval by the ethics committee of the Xijing Hospital (No. approval number:

XJYYLL-2015625). Mice feeding, housing, and handling were conducted in strict adherence to local regulations and after approval by the animal ethics committee of the Fourth Military Medical University (No. 20240720).

**Consent for publication**
Not applicable.

**Competing interests**
The authors declare that they have no competing interests.

**Author details**
[1]State Key Laboratory of Holistic Integrative Management of Gastrointestinal Cancers, National Clinical Research Center for Digestive Diseases and Xijing Hospital of Digestive Diseases, Fourth Military Medical University, Xi'an 710032, China. [2]State Key Laboratory of Holistic Integrative Management of Gastrointestinal Cancers, Department of Biochemistry and Molecular Biology, Fourth Military Medical University, Xi'an 710032, China. [3]Department of Gastrointestinal Surgery, Xijing Hospital, Fourth Military Medical University, Xi'an 710032, China. [4]Department of General Surgery, Central Theater Command General Hospital of the Chinese People's Liberation Army, Wuhan 430070, China. [5]Department of Thoracic Surgery, Tangdu Hospital, Fourth Military Medical University, Xi'an 710000, China. [6]Henan Key Laboratory of Immunology and Targeted Therapy, School of Laboratory Medicine, Xinxiang Medical University, Xinxiang 453003, China. [7]School of Clinical Medicine, Xi'an Medical University, Xi'an 710000, China. [8]Department of Experimental Surgery, Xijing Hospital, Fourth Military Medical University, Xi'an 710032, China. [9]CAS Key Laboratory of Infection and Immunity, Institute of Biophysics, National Laboratory of Biomacromolecules, CAS Center for Excellence in Biomacromolecules, Chinese Academy of Sciences, Beijing 100101, China. [10]The Ministry of Education Key Lab of Hazard Assessment and Control in Special Operational Environment, Fourth Military Medical University, Xi'an 710032, China. [11]State Key Laboratory of Holistic Integrative Management of Gastrointestinal Cancers, Department of Immunology, Fourth Military Medical University, Xi'an 710032, China.

Received: 7 April 2024 Accepted: 5 March 2025
Published online: 23 March 2025

**References**

1. Hyuna S, Jacques F, Rebecca LS, Mathieu L, Isabelle S, Ahmedin J, Freddie B. Global cancer statistics 2020: GLOBOCAN estimates of incidence and mortality worldwide for 36 cancers in 185 countries. CA Cancer J Clin. 2021;71:209.
2. Ally A, Balasundaram M, Carlsen R, Chuah E, Clarke A, Dhalla N, Holt RA, Jones S, Lee D, Ma Y, et al. Comprehensive and Integrative Genomic Characterization of Hepatocellular Carcinoma. Cell. 2017;169:1327–1341.e1323.
3. Hlady RA, Robertson KD. Genetic and epigenetic heterogeneity in normal liver homeostasis and its implications for liver disease and hepatocellular cancer. Semin Liver Dis. 2018;38:41–50.
4. Llovet JM, Montal R, Sia D, Finn RS. Molecular therapies and precision medicine for hepatocellular carcinoma. Nat Rev Clin Oncol. 2018;15:599–616.
5. Sohum M, Jin Z. Liquid-liquid phase separation drives cellular function and dysfunction in cancer. Nat Rev Cancer. 2022;22:239–52.
6. Jeong-Mo C, Alex SH, Rohit VP. Physical principles underlying the complex biology of intracellular phase transitions. Annu Rev Biophys. 2020;49:107.
7. Hnisz D, Shrinivas K, Young R, Chakraborty A, Sharp P. A phase separation model for transcriptional control. Cell. 2017;169:13–23.
8. Bouchard J, Otero J, Scott D, Szulc E, Martin E, Sabri N, Granata D, Marzahn M, Lindorff-Larsen K, Salvatella X, et al. Cancer mutations of the tumor suppressor SPOP disrupt the formation of active. Phase-Separated Compartments Molecular cell. 2018;72:19-36.e18.
9. Trojanowski J, Frank L, Rademacher A, Mücke N, Grigaitis P, Rippe K. Transcription activation is enhanced by multivalent interactions independent of phase separation. Mol Cell. 2022;82:1878-1893.e1810.
10. Boija A, Klein I, Sabari B, Dall'Agnese A, Coffey E, Zamudio A, Li C, Shrinivas K, Manteiga J, Hannett N, et al. Transcription factors activate genes through the phase-separation capacity of their activation domains. Cell. 2018;175:1842-1855.e1816.
11. Zhang H, Shao S, Zeng Y, Wang X, Qin Y, Ren Q, Xiang S, Wang Y, Xiao J, Sun Y. Reversible phase separation of HSF1 is required for an acute transcriptional response during heat shock. Nat Cell Biol. 2022;24:340–52.
12. Liu J, Chen Y, Nong B, Luo X, Cui K, Li Z, Zhang P, Tan W, Yang Y, Ma W, et al. CRISPR-assisted transcription activation by phase-separation proteins. Protein Cell. 2023;14:874–87.
13. Liu Q, Li J, Zhang W, Xiao C, Zhang S, Nian C, Li J, Su D, Chen L, Zhao Q, et al. Glycogen accumulation and phase separation drives liver tumor initiation. Cell. 2021;184:5559-5576.e5519.
14. Laoukili J, Kooistra MR, Brás A, Kauw J, Kerkhoven RM, Morrison A, Clevers H, Medema RH. FoxM1 is required for execution of the mitotic programme and chromosome stability. Nat Cell Biol. 2005;7:126–36.
15. Hannenhalli S, Kaestner KH. The evolution of Fox genes and their role in development and disease. Nat Rev Genet. 2009;10:233–40.
16. Bella L, Zona S, Nestal de Moraes G, Lam EW. FOXM1: a key oncofoetal transcription factor in health and disease. Semin Cancer Biol. 2014;29:32–9.
17. Weiler SME, Pinna F, Wolf T, Lutz T, Geldiyev A, Sticht C, Knaub M, Thomann S, Bissinger M, Wan S, et al. Induction of chromosome instability by activation of yes-associated protein and forkhead box M1 in liver cancer. Gastroenterology. 2017;152:2037-2051.e2022.

18. Chai N, Xie HH, Yin JP, Sa KD, Guo Y, Wang M, Liu J, Zhang XF, Zhang X, Yin H, et al. FOXM1 promotes proliferation in human hepatocellular carcinoma cells by transcriptional activation of CCNB1. Biochem Biophys Res Commun. 2018;500:924–9.
19. Liu J, Li J, Wang K, Liu H, Sun J, Zhao X, Yu Y, Qiao Y, Wu Y, Zhang X, et al. Aberrantly high activation of a FoxM1-STMN1 axis contributes to progression and tumorigenesis in FoxM1-driven cancers. Signal Transduct Target Ther. 2021;6:42.
20. Bond J, Roberts E, Mochida GH, Hampshire DJ, Scott S, Askham JM, Springell K, Mahadevan M, Crow YJ, Markham AF, et al. ASPM is a major determinant of cerebral cortical size. Nat Genet. 2002;32:316–20.
21. Bond J, Scott S, Hampshire D, Springell K, Corry P, Abramowicz M, Mochida G, Hennekam R, Maher E, Fryns J, et al. Protein-truncating mutations in ASPM cause variable reduction in brain size. Am J Hum Genet. 2003;73:1170–7.
22. Wu X, Xu S, Wang P, Wang ZQ, Chen H, Xu X, Peng B. ASPM promotes ATR-CHK1 activation and stabilizes stalled replication forks in response to replication stress. Proc Natl Acad Sci U S A. 2022;119: e2203783119.
23. Lin S, Pan H, Liu S, Jeng Y, Hu F, Peng S, Lai P, Hsu H. ASPM is a novel marker for vascular invasion, early recurrence, and poor prognosis of hepatocellular carcinoma. Clin Cancer Res. 2008;14:4814–20.
24. Hsu CC, Liao WY, Chang KY, Chan TS, Huang PJ, Chiang CT, Shan YS, Cheng LH, Liao TY, Tsai KK. A multi-mode Wnt- and stemness-regulatory module dictated by FOXM1 and ASPM isoform I in gastric cancer. Gastric Cancer. 2021;24:624–39.
25. Wang WY, Hsu CC, Wang TY, Li CR, Hou YC, Chu JM, Lee CT, Liu MS, Su JJ, Jian KY, et al. A gene expression signature of epithelial tubulogenesis and a role for ASPM in pancreatic tumor progression. Gastroenterology. 2013;145:1110–20.
26. Pai VC, Hsu CC, Chan TS, Liao WY, Chuu CP, Chen WY, Li CR, Lin CY, Huang SP, Chen LT, Tsai KK. ASPM promotes prostate cancer stemness and progression by augmenting Wnt-Dvl-3-β-catenin signaling. Oncogene. 2019;38:1340–53.
27. Zeng WJ, Cheng Q, Wen ZP, Wang JY, Chen YH, Zhao J, Gong ZC, Chen XP. Aberrant ASPM expression mediated by transcriptional regulation of FoxM1 promotes the progression of gliomas. J Cell Mol Med. 2020;24:9613–26.
28. Hsu CC, Liao WY, Chan TS, Chen WY, Lee CT, Shan YS, Huang PJ, Hou YC, Li CR, Tsai KK. The differential distributions of ASPM isoforms and their roles in Wnt signaling, cell cycle progression, and pancreatic cancer prognosis. J Pathol. 2019;249:498–508.
29. Liao WY, Hsu CC, Chan TS, Yen CJ, Chen WY, Pan HW, Tsai KK. Dishevelled 1-regulated superpotent cancer stem cells mediate Wnt heterogeneity and tumor progression in hepatocellular carcinoma. Stem Cell Rep. 2020;14:462–77.
30. Bernhofer M, Goldberg T, Wolf S, Ahmed M, Zaugg J, Boden M, Rost B. NLSdb-major update for database of nuclear localization signals and nuclear export signals. Nucleic Acids Res. 2018;46:D503-d508.
31. Fu Z, Malureanu L, Huang J, Wang W, Li H, van Deursen J, Tindall D, Chen J. Plk1-dependent phosphorylation of FoxM1 regulates a transcriptional programme required for mitotic progression. Nat Cell Biol. 2008;10:1076–82.
32. Anders L, Ke N, Hydbring P, Choi Y, Widlund H, Chick J, Zhai H, Vidal M, Gygi S, Braun P, Sicinski P. A systematic screen for CDK4/6 substrates links FOXM1 phosphorylation to senescence suppression in cancer cells. Cancer Cell. 2011;20:620–34.
33. Lafontaine D, Riback J, Bascetin R, Brangwynne C. The nucleolus as a multiphase liquid condensate. Nat Rev Mol Cell Biol. 2021;22:165–82.
34. Ahn J, Davis E, Daugird T, Zhao S, Quiroga I, Uryu H, Li J, Storey A, Tsai Y, Keeley D, et al. Phase separation drives aberrant chromatin looping and cancer development. Nature. 2021;595:591–5.
35. Xie Z, Janczyk P, Zhang Y, Liu A, Shi X, Singh S, Facemire L, Kubow K, Li Z, Jia Y, et al. A cytoskeleton regulator AVIL drives tumorigenesis in glioblastoma. Nat Commun. 2020;11:3457.
36. Chen Z, Hou C, Wang L, Yu C, Chen T, Shen B, Hou Y, Li P, Li T. Screening membraneless organelle participants with machine-learning models that integrate multimodal features. Proc Natl Acad Sci USA. 2022;119: e2115369119.
37. Jumper J, Evans R, Pritzel A, Green T, Figurnov M, Ronneberger O, Tunyasuvunakool K, Bates R, Žídek A, Potapenko A, et al. Highly accurate protein structure prediction with AlphaFold. Nature. 2021;596:583–9.
38. Abramson J, Adler J, Dunger J, Evans R, Green T, Pritzel A, Ronneberger O, Willmore L, Ballard A, Bambrick J, et al. Accurate structure prediction of biomolecular interactions with AlphaFold 3. Nature. 2024;630:493–500.
39. Ye H, Holterman AX, Yoo KW, Franks RR, Costa RH. Premature expression of the winged helix transcription factor HFH-11B in regenerating mouse liver accelerates hepatocyte entry into S phase. Mol Cell Biol. 1999;19:8570–80.
40. Wang X, Quail E, Hung NJ, Tan Y, Ye H, Costa RH. Increased levels of forkhead box M1B transcription factor in transgenic mouse hepatocytes prevent age-related proliferation defects in regenerating liver. Proc Natl Acad Sci U S A. 2001;98:11468–73.
41. Hodgson JG, Yeh RF, Ray A, Wang NJ, Smirnov I, Yu M, Hariono S, Silber J, Feiler HS, Gray JW, et al. Comparative analyses of gene copy number and mRNA expression in glioblastoma multiforme tumors and xenografts. Neuro Oncol. 2009;11:477–87.
42. Liao GB, Li XZ, Zeng S, Liu C, Yang SM, Yang L, Hu CJ, Bai JY. Regulation of the master regulator FOXM1 in cancer. Cell Commun Signal. 2018;16:57.
43. Kopanja D, Pandey A, Kiefer M, Wang Z, Chandan N, Carr J, Franks R, Yu D, Guzman G, Maker A, Raychaudhuri P. Essential roles of FoxM1 in Ras-induced liver cancer progression and in cancer cells with stem cell features. J Hepatol. 2015;63:429–36.
44. Xia L, Huang W, Tian D, Zhu H, Zhang Y, Hu H, Fan D, Nie Y, Wu K. Upregulated FoxM1 expression induced by hepatitis B virus X protein promotes tumor metastasis and indicates poor prognosis in hepatitis B virus-related hepatocellular carcinoma. J Hepatol. 2012;57:600–12.
45. Man Y, Zhengxin P, Min Q, Yang L, Jingning W, Cai Z, Jiaming L, Tianqi D, Lulu W, Shasha L, et al. Interferon-γ induces tumor resistance to anti-PD-1 immunotherapy by promoting YAP phase separation. Mol Cell. 2021;81:1216-1230.e9.
46. Bappaditya C, Nicole LM, Hazheen KS, Swarnendu T, Brittany JP, David WB, Diana MM, Ilaria I, Michael RW, Jingjing C, et al. Phase separation mediates NUP98 fusion oncoprotein leukemic transformation. Cancer Discov. 2021;12:1152–69.
47. Wakefield JG, Bonaccorsi S, Gatti M. The drosophila protein asp is involved in microtubule organization during spindle formation and cytokinesis. J Cell Biol. 2001;153:637–48.

48. Kouprina N, Pavlicek A, Collins NK, Nakano M, Noskov VN, Ohzeki J, Mochida GH, Risinger JI, Goldsmith P, Gunsior M, et al. The microcephaly ASPM gene is expressed in proliferating tissues and encodes for a mitotic spindle protein. Hum Mol Genet. 2005;14:2155–65.
49. Luo G, Lin X, Vega-Medina A, Xiao M, Li G, Wei H, Velázquez-Martínez CA, Xiang H. Targeting of the FOXM1 oncoprotein by E3 ligase-assisted degradation. J Med Chem. 2021;64:17098–114.
50. Chen Y, Yang C, Huang J, Wang P, Lv Y, Tang C, Deng W. An introduction of an easy-operating and economical technique for tissue microarray preparation. J Clin Pathol. 2020;73:403–7.
51. Comeau S, Gatchell D, Vajda S, Camacho C. ClusPro: a fully automated algorithm for protein-protein docking. Nucleic Acids Res. 2004;32:W96-99.
52. Adasme M, Linnemann K, Bolz S, Kaiser F, Salentin S, Haupt V, Schroeder M. PLIP 2021: expanding the scope of the protein-ligand interaction profiler to DNA and RNA. Nucleic Acids Res. 2021;49:W530–4.
53. Gao X, Xia X, Li F, Zhang M, Zhou H, Wu X, Zhong J, Zhao Z, Zhao K, Liu D, et al. Circular RNA-encoded oncogenic E-cadherin variant promotes glioblastoma tumorigenicity through activation of EGFR-STAT3 signalling. Nat Cell Biol. 2021;23:278–91.
54. Roessler S, Long E, Budhu A, Chen Y, Zhao X, Ji J, Walker R, Jia H, Ye Q, Qin L, Tang Z, He P, Hunter K, Thorgirsson S, Meltzer P, Wang X. Gene expression data of human hepatocellular carcinoma (HCC). RNA-sequencing datasets. Gene Expression Omnibus. 2010. https://www.ncbi.nlm.nih.gov/geo/query/acc.cgi?acc=GSE14520.
55. Wurmbach E, Chen Y, Khitrov G, Zhang W, Roayaie S, Schwartz M, Fiel I, Thung S, Mazzaferro V, Bruix J, Bottinger E, Friedman S, Waxman S, Llovet J. Genome-wide molecular profiles of HCV-induced dysplasia and hepatocellular carcinoma. RNA-sequencing datasets. Gene Expression Omnibus. 2007. https://www.ncbi.nlm.nih.gov/geo/query/acc.cgi?acc=GSE6764.
56. Liu Y. ASPM mediates nuclear entrapment of FOXM1 via liquid-liquid phase separation to promote progression of hepatocarcinoma. Github. 2025. https://github.com/ykliu2025/liu_250208.
57. Liu Y. ASPM mediates nuclear entrapment of FOXM1 via liquid-liquid phase separation to promote progression of hepatocarcinoma. Zenodo. 2025. https://doi.org/10.5281/zenodo.14835716.

## Publisher's Note